Ignition of natural fuels from strikes between steel and rocks

Johan Sjöström
Michael Försth
Paul Otoxorena
Robert Svensson

BRAND
FORSK

Reference group

Mattias Delin, Brandforsk
Leif Sandahl, The Swedish Civil Contingencies Agency, MSB
Tomas Johannesson, Skogsforsk

Abstract

Ignition of natural fuels from strikes between steel and rocks

The ignition of natural fuels by sparks from strikes between metals and hard rock is far from understood and the ignition potential of sparks from rock strikes during heavy machinery operations is disputed in the scientific literature. This study utilises a spectrally resolved technique to study the temperature evolution of metal sparks from rock strikes. The study shows that initial temperature after collision can easily reach 1500 °C and this temperature can increase additionally by several hundred degrees as rapid oxidation processes are initiated, often leading to further disintegration of the fragment. The average temperature of fragments from such collisions is here measured to 1400 – 2000 °C and the combination of temperature, size and exothermic processes makes them viable for forest litter igniting. However, ignition on forest lands is always an unlikely, although possible outcome of heavy machinery operations and should be considered in risk assessment of the activity.

Key words: Ignition, sparks, stone, metal, forestry, wildfire

Content

Summary

This study investigates the size- and temperature evolution of spark from strikes between steel and hard rocks since previous research have different conclusion of the possibility for such sparks to ignite forest litter. The sparks investigated here are metal fragments parting from the mother material in the collision with hard rocks (granite of flint). We describe a technique using a grating spectrometer coupled to a fast detector with a spectral response ranging from 300 to 1000 nm to measure temperatures of fragments. This technique eliminates problems of cold background pixel averaging, moving particles during exposure and unknown emissivity that comes with i.e., IR camera imaging.
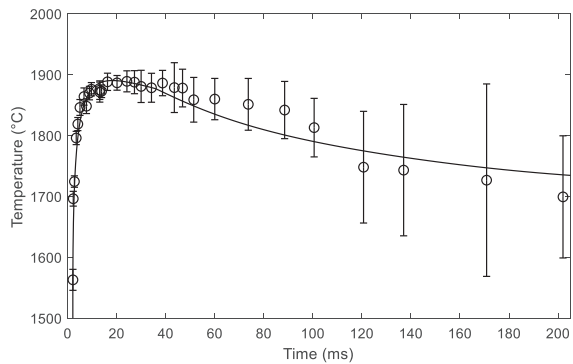
Temperature evolution of Hardox metal fragments (Figure 26).

The study shows that during the deformation process as fragments part from the mother material the temperature of the fragment can easily reach 1500 °C. At such temperature, a rapid oxidation process occurs, further increasing fragment temperatures up to several hundred degrees. The increasing temperature can lead to disintegration of fragments leading to further oxidation and a fast heat loss to the surrounding.

This is intentionally utilised in modern fire steel products, but is also a common process in fragments from collisions between tough steel and hard rock. The temperature of fragments from such collisions is here measured to 1400 - 2000 °C and the combination of temperature, size and exothermic processes makes them viable for forest litter igniting. However, ignitions on forest lands also require both specific fuel conditions and spark trajectory ending in a fuel environment beneficial for ignition and growth.
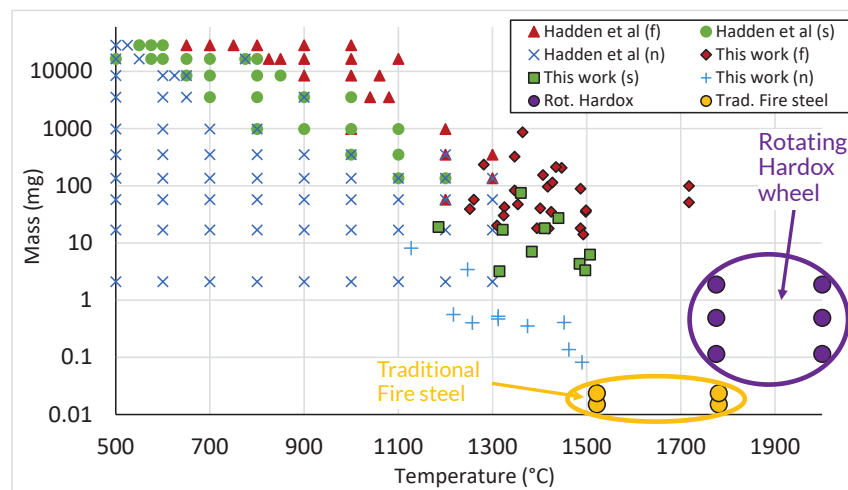
Mass and temperature of metal fragments and their potential to ignite α-cellulose or sawdust (Figure 28).

Sammanfattning

Storleks- och temperaturutveckling på gnistor från kollisioner mellan hårdstål och stenmaterial har studerats för att utvärdera dess potential att antända skogsförna, något som tidigare studier drar olika slutsatser om. Gnistorna som studeras är metallfragment från kollisioner med granit eller flinta. Spektrometri har använts för att studera temperaturutvecklingen hos olika typer av gnistor. Tekniken lider inte av pixelmedelvärdesbildning med kall bakgrund, partiklar i snabb rörelse under exponering, eller av okänd emissivitet såsom är fallet för exempelvis IR-kameratekniker.

Resultaten visar att metallfragmenten under deformationen i kollisionen kan uppnå temperaturer på omkring 1500 °C. Vid dessa temperaturer initieras en snabb oxideringsprocess vilken i sin tur kan öka temperaturen ytterligare flera hundra °C. Den ökande temperaturen kan leda till vidare fragmentering av partikeln i mindre bitar med ökad oxidering och värmeförlust till omgivningen.

Temperaturutveckling av metallfragment från Hardoxstål (Figure 26).

Denna process utnyttjas i moderna tändstål men förekommer även för gnistor från kollisioner mellan hårdstål och stenar. Gnisttemperaturen från sådana kollisioner mäts i denna studie till mellan 1400 och 2000 °C och kombinationen av temperatur, storlek och exoterma processer gör gnistorna potenta nog att antända skogsförna. Antändning ute i markerna kräver dock både specifika bränsleförutsättningar och gnistor som vars bana är sådan att den landar i en omgivning lokal omgivning där antändning kan ske och växa.
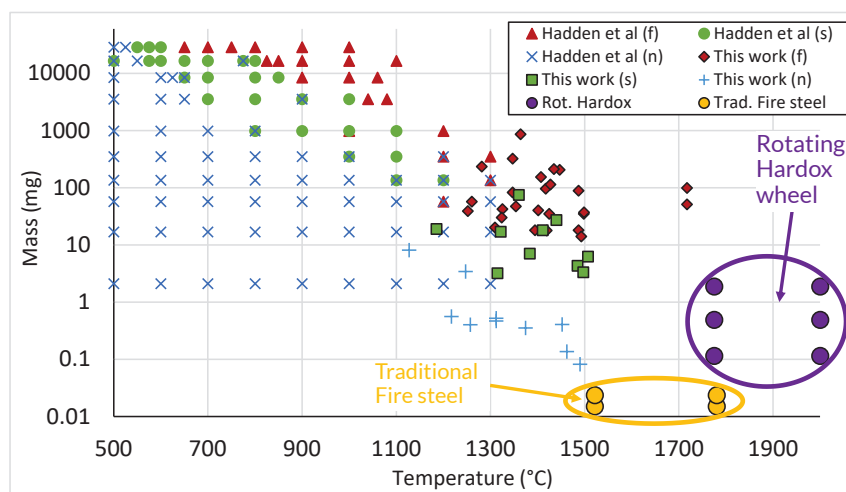
Massa och temperatur av metallfragment och deras potential att antända cellulosa och sågspån (Figure 28).

1 Background

Statements such as [… *a spark ignited the fuel* …] is commonly occurring in descriptions of fires but this is a highly general term for a number of different actions such as electrical discharge over small distances (Ochoterena & Försth, 2014), welding particles and fumes (Omar et al, 2007), hot metal particles from friction (Mikkelsen, 2014), rapidly oxidizing particles (Zarko & Glazunov, 2020), burning embers (Viegas et al, 2014) or disposal of ashes containing smouldering materials (Shelton, 1979). These processes all represent different avenues for obtaining ignition and they all exhibit specific requirements for both "spark" and fuel for the success of such ignition. The actual physical mechanisms behind hot particle ignition, which comprise all phenomena above except electric discharge, is highly complex and therefore literature more commonly refers to the probability of ignition rather than precise requirements (Fernandez-Pello, 2017).

That sparks (fragments) from strikes between metal and rock can ignite combustible material is well known, old examples include the flintlock on old firearms as well as flint and steel to start campfires. During recent years products metal-metal strikes involving highly oxidating alkali metals or lanthanides have also grown in popularity for their easy igniting of natural fuels.

1.1 Wildfire ignition

If ignition from hot particles generally constitute complex phenomena the application to wildfire ignition, and thus ignition of vegetation fuels, is even more complex due to the large heterogeneity and complexity of natural fuels beds.

Wildfire ignition is to more than 90 % anthropogenic. Thus, the origin is due to accidents, deliberate actions or negligence by humans (Stanley et al, 2020). In most regions lightning (virtually the only non-anthropogenic wildfire ignition source) accounts for only a small fraction of registered ignitions and anthropogenic fires for at least 84 % of ignitions (North America; Balch et al, 2017), to more commonly 95 % (California; Cal Fire, 2015), 96 % (Victoria, Australia; Bryant, 2008) and 93 % (of known causes, Sweden; Sjöström & Granström, 2020). In most areas the anthropogenic fires lead to a significantly prolonged fire season (e.g. a factor 3) and about twice the burnt area (Balch et al, 2017).

Among the human-caused fires different causes of ignition lead to different types of fires (in terms of fuels and burnt area). Whereas arson, children playing with fire, and debris burning in gardens often spread in light fuels and cause small burnt area in Sweden, reignition of previously contained fires, disposal of ashes, powerline failure and "other sparks" contribute more to forest fires burning relatively large areas. Generally, wildfire occurrence in Sweden (and most other regions) is highly correlated to population density whereas the larger fires usually occur further from densely populated areas due to the prolonged time to detection and initial attack as well as poorer mop-up (Sjöström & Granström, 2020).

Even though one can describe ignition of vegetation fuels on large statistical data sets each individual ignition is associated to very large uncertainties. The forest fuel is highly heterogeneous as is a successful ignition of a spark, pilot flame or alike. Local phenomena

such as shading, southern/northern slopes soil fertilities affect the possibilities of fuel whereas the microscopic variations such as fuel density, wind exposure and orientation have huge impacts which are far from understood.

1.1.1   Ignitions related to forestry activities

Ignition from forestry activities, and more specifically from heavy machinery, have raised significant attention in Sweden during the last decade or more. This is primarily due to a few large and high-impact incidents directly ignited by forwarding or scarification (site preparation). These include the 1 900 ha large fire in Bodträskfors 2006 (Boden's Municipality, 2006) and the infamous 13 000 ha Västmanland fire 2014 (MSB, 2015). Due to this attention, ignitions from forestry machinery in Sweden was studied in detail and from a review of incidents leading to rescue service dispatch (1998-2015) and machine operator interviews the annual average of ignitions from forestry machinery was estimated to 220 – 480, with about 10 % leading to fire-fighting dispatch. Most ignitions originated from scarification (site preparation before sowing/planting). The geographical pattern of ignitions correlated strongly with the occurrence of large rocks in the landscape (Sjöström et al, 2019).

After the increased attention, routines and guidelines for consultation between contractors, operators and landowner were agreed on within the industry to strengthen preparedness and clarify responsibilities (Skogforsk, 2017).

Figure 1. Left: overview of a scarifier use for site preparation. Right: photo from below the machine showing the protection plate, the bogie and the wheel tracks on an extruding rock.

A reporting effort from land managers to Skogforsk covered ~50 % of all clear-felled area between 2018-2019. From this dataset the occurrence of fires ignited from forestry machinery was 87 for the two years, constituting 1.1 and 1.4 % of all forest fires 2018 and 2019, respectively (but only 0.7 % of all ignitions including grass fires) (Hyll et al, 2020). This is less than that estimated from 1998 – 2015 indicating that the guidelines set in place by the industry has helped raising knowledge and awareness. Interestingly, the forestry action resulting in most ignition was forwarding, and not scarification and the main involved machinery part was the wheel tracks used outside the rubber wheels for sliding protection. 2nd most common part was the protection steel under the machine combined with the bogie and scarification disc only at 3rd place (Hyll et al, 2020). The ignition from metal contact with rock or other metal is however not limited to forestry actions. Faulty breaks or alike on trains cause a number of fires annually as do operations of grass and bush cutters along roadsides (Sjöström & Granström, 2020).

The question of limitations and requirements for hot particle ignition from hot steel is highly relevant for many industrial fields. The literature on the subject is however very scarce but a study on metal fragments from bulldozers running over rocky terrain under extreme conditions used infrared video recordings concluded that such fragments are *not* a viable source of ignition of forest litter (Howitt, 2015). The conclusion is drawn based on the IR imaging measurements showing that the fragments from the strikes are less than 500 °C in all but one occurrence and that the temperatures after 1 s all have decreased to below 400 °C. These temperatures, compared to studies on heated metal spheres dropped onto dry α-cellulose concludes that the sparks do not exhibit the potential for igniting organic materials, something that contrasts the examples of spark ignitions discussed above. The temperatures from these sparks are, however, very low compared to the colour of typical sparks from metal/rock strikes, see below.

1.2 Theory of ignition by hot particles

In this section a holistic description of ignition by metal particles is given. For a complete picture the mechanisms determining the temperature of the particle is required, as a prerequisite to the physicochemical processes occurring when metal particles of different sizes and temperatures land in a fuel bed.

1.2.1 Temperature history of a hot particle

The final temperature of a metal particle impinging on the fuel has contributions from three phases. Firstly, when the particle is mechanically ejected from the bulk metal a large fraction of the collision energy is transformed into heat. Secondly, once ejected the particle will expose un-oxidized metal surfaces to the oxygen in the air and exothermic oxidation processes will heat up the particle further. Thirdly and finally, there will be convective and radiative heat losses to the surroundings during the particle's trajectory to the fuel bed. These processes are described in some detail in this section.

1.2.1.1 Initial temperature

Metal shavings are formed when a metallic element translating at high velocity impinges onto a hard material, such as a flint- or granite stone. A portion of the metallic object is removed by shear deformation, forming a metal chip (Figure 2). A metallic object with a velocity v collides partially with a stone and the collision event results in the formation of a fragment (or shaving) with a thickness dt.
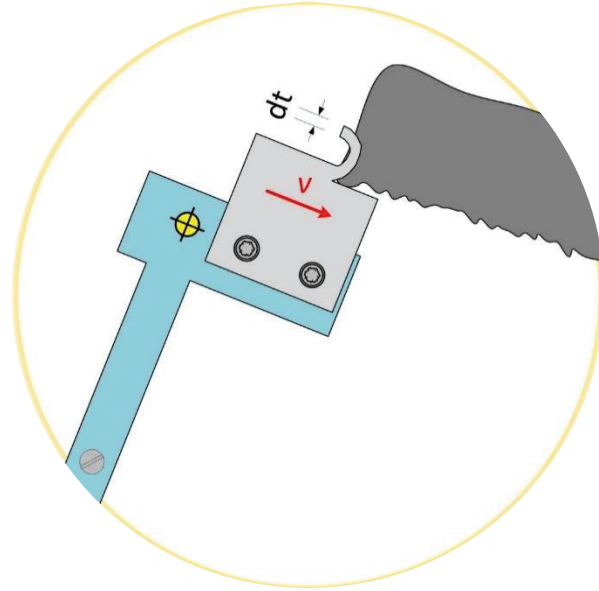
Figure 2. Metallic object impinging on a rock material.

If the collision does not result in other plastic deformations of the metallic element nor fractures in the stone material, but solely on the formation of metal shavings, approximately 98 % of the energy of the collision is converted into heat (Shaw, 1985). The increment in temperature of the shavings, ΔT (K) can be estimated by dimensional analysis, where factors such as the specific energy of the material, u (J/kg), the translational speed of the impinging metallic object, v (m/s), the thickness of the shaving, dt (m), the thermal diffusivity of work material, K (m²/s), and the volumetric specific heat of the metal, ρC (J/m³K), are considered.

Combining the aforementioned factors results in Equation (1) (Merchant, 1945; Finnie, 1956), where a proportionality coefficient equal to 0.4, known as the Cook coefficient, is employed (Cook, 1966).

$$\Delta T = \frac{0.4\,u}{\rho\,C}\left(\frac{v\,dt}{K}\right)^{1/3} \qquad (1)$$

Computed increments in temperature for shavings from three metallic materials as a function of deformation speed and for two thicknesses of shavings, dt, are plotted in Figure 3. The materials are High Carbon Steel AISI 1095, Stainless Steel 304 and Hardox 450. For collisions with speeds between 0-5 and 1 m/s the temperature increase of the shaving is well over 1000 °C for a 250 µm thick shaving and over 1400 °C for a 100 µm thick one. Additionally, with increasing hardness of the steel the temperature increases (Figure 3).
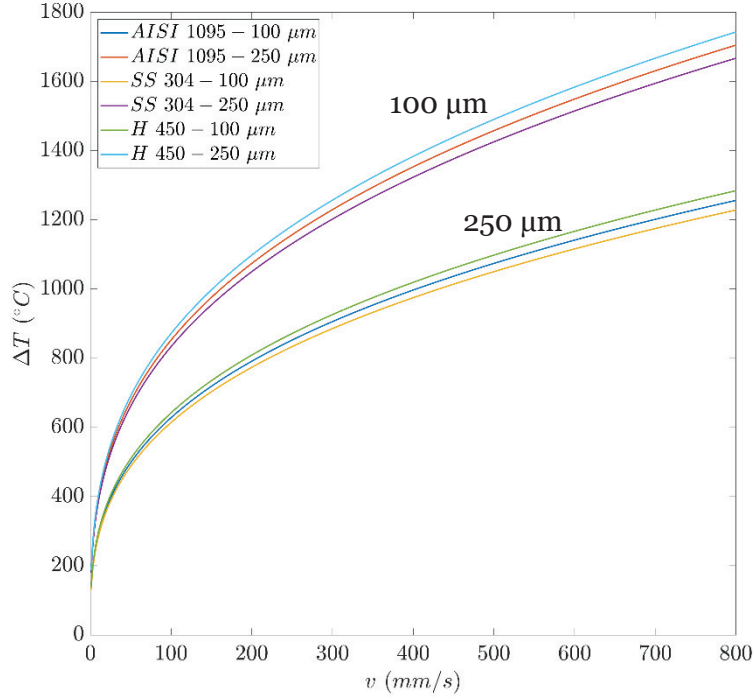
Figure 3. Temperature increment of shavings from three metallic materials as a function of deformation speed and for two thicknesses according to Equation (1).

1.2.1.2 Heating

When a metal particle is emitted from a bigger piece of metal, virgin un-oxidized metal surfaces are exposed to the oxygen in the air. An example is when flint is used to hit carbon steel, and small carbon steel particles is emitted into the air. The fresh metal surface becomes oxidized, with the oxidation rate strongly depending on the metal type as well as the temperature of the metal surface. A graph of the temperature dependence of iron oxidation is shown in the appendix describing the huge differences in oxidation rates between 500 and 1500 °C (Figure 35). A most relevant example is again high carbon steel. High carbon steel is brittle, allowing for relatively easy detachment of metal fragments. The iron in the exposed surfaces will quickly oxidize, in other words it rusts, fast. The oxidation process is exothermic and will heat up the particle. If the particle is small enough the surface-to-volume ratio will be high enough to heat up the particles enough that they start to glow. Thus, the blackbody radiation from the particle will be intense enough for the human eye to see. Also, the color of the glowing particle will depend on its temperature, which can be used for temperature assessment. The color experienced by the human eye depends on the distribution of the blackbody radiation in a relatively complex way. However, the wavelength with maximum radiation for a given temperature is easily expressed by Wien's displacement law.

$$\lambda_{peak} = \frac{b}{T} \qquad (2)$$

Where $b = 2.9 \cdot 10^{-3}$ m·K is Wien's displacement constant and T in Kelvin. Heating of the metal particle will stop when the heat losses, the cooling, overcomes the exothermic oxidation heat. The oxidation rate is in itself temperature dependent as described above, such that the time when heating stops will depend on many parameters, such as particle size and shape, surface roughness, etc.

1.2.1.3   Cooling

Heat losses from a hot particle to its surrounding environment takes place via convection and radiation. Conduction in the air also plays a role but is typically considered as a part of convection, where the convective heat transfer coefficient as calculated based on heat conduction in the boundary layer close to the surface. Radiative losses from a surface, also called exitance, is given by the Stefan-Boltzmann law adjusted for the emissivity ε of the surface

$$\dot{q}^{"} = \varepsilon \sigma T^4 \tag{3}$$

Where $\sigma = 5.67 \cdot 10^{-8}$ W·m⁻²·K⁻⁴ is the Stefan-Boltzmann. The T^4-dependence implies that radiative cooling is most significant and fastest when the particle temperature is high. In reality the emissivity is spectrally dependent, meaning that surfaces do not generally exhibit the same emissivity for all wavelengths. The spectrally resolved exitance from a surface into vacuum is given by the Planck radiation law

$$\dot{q}^{"}_\lambda = \frac{2\pi \varepsilon_\lambda h c_0^2}{\lambda^5 \left[exp\left(\frac{hc_0}{n\lambda k_B T}\right) - 1 \right]} \tag{4}$$
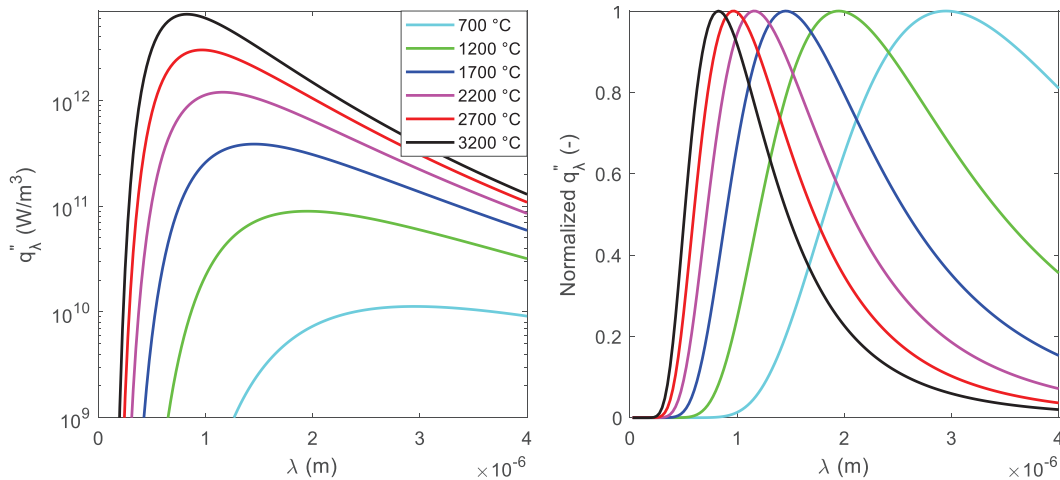

Figure 4. Spectrally resolved emittance from black bodies of different temperatures. (left): actual emittance per unit area, (right) normalized emittance on a linear y-axis.

Where $h = 6.6 \cdot 10^{-34}$ J·s is Planck's constant, $c_0 = 3.0 \cdot 10^8$ m·s⁻¹ is the speed of light in vacuum, $k_B = 1.38 \cdot 10^{-23}$ J·K⁻¹ is the Boltzmann constant and T the black body temperature in Kelvin. In fact, the Stefan Boltzmann law, Eq. *(3)*, is the Planck law, Eq. *(4)* integrated over all wavelengths. Eq. *(4)* and *(3)* imply that the emissivity plays an

important role for the radiative cooling rate and some studies of its behavior for hot metal particles is therefore presented here.

The spectral emissivity obviously depends on wavelength, but also on temperature (Shi et al, 2014). The spectral emissivity may also depend on surface roughness (Otsuka et al, 2005; Sabuga & Todtenhaupt, 2001; Wen & Mudawar, 2004, 2005), mission angle (Campo et al, 2006; Furukawa & Iuchu, 2000) and oxidization film on its surface (Kobayashi et al, 1999; Punjana et al, 2007; Shi et al, 2014). Specifically, a material such as steel at an elevated temperature undergoes surface oxidization while travelling in air.

The surface oxidization usually increases the spectral emissivity of a metallic surface that is maintained at an elevated temperature. An example of this increase is shown in Figure 5 where Shi et al. used a, InGaAs photodiode detector to measure emitted radiation from steel 304 heated to 1100 K. The spectral emissivity increases rapidly upon heating but then flattens out and stabilizes at around 0.79, which is an increase of approximately 5 % as compared to the original spectral emissivity of 0.75. Although the increasing trend is very clear it can also be noticed that the final spectral emissivity do not deviate more than 5 % as compared to the original value which is similar to the increase in emissivity previously measured on brass by the same group (Shi et al, 2014).
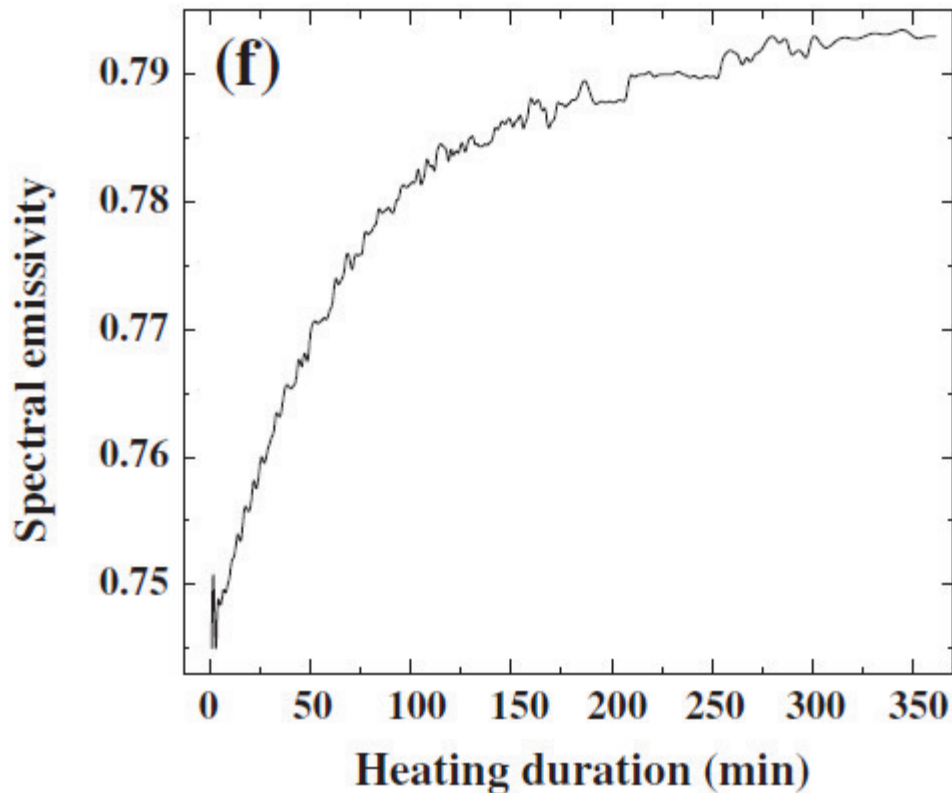

Figure 5. Increase in spectral emissivity, at 1.5 μm, for steel 304 heated to 1100 K (Shi, Zou, et al., 2014).

Figure 6 shows the temperature dependence on the spectral emissivity for steel 304. As can be seen the increase in spectral emissivity is quite substantial increasing by almost 25 % from 0.63 to 0.78 in a temperature interval of 850 K to 1100 K (Shi, Zou, et al.,

2014), which is a relatively narrow temperature interval as compared to the temperature development that can be expected from a glowing particle being cooled in air.
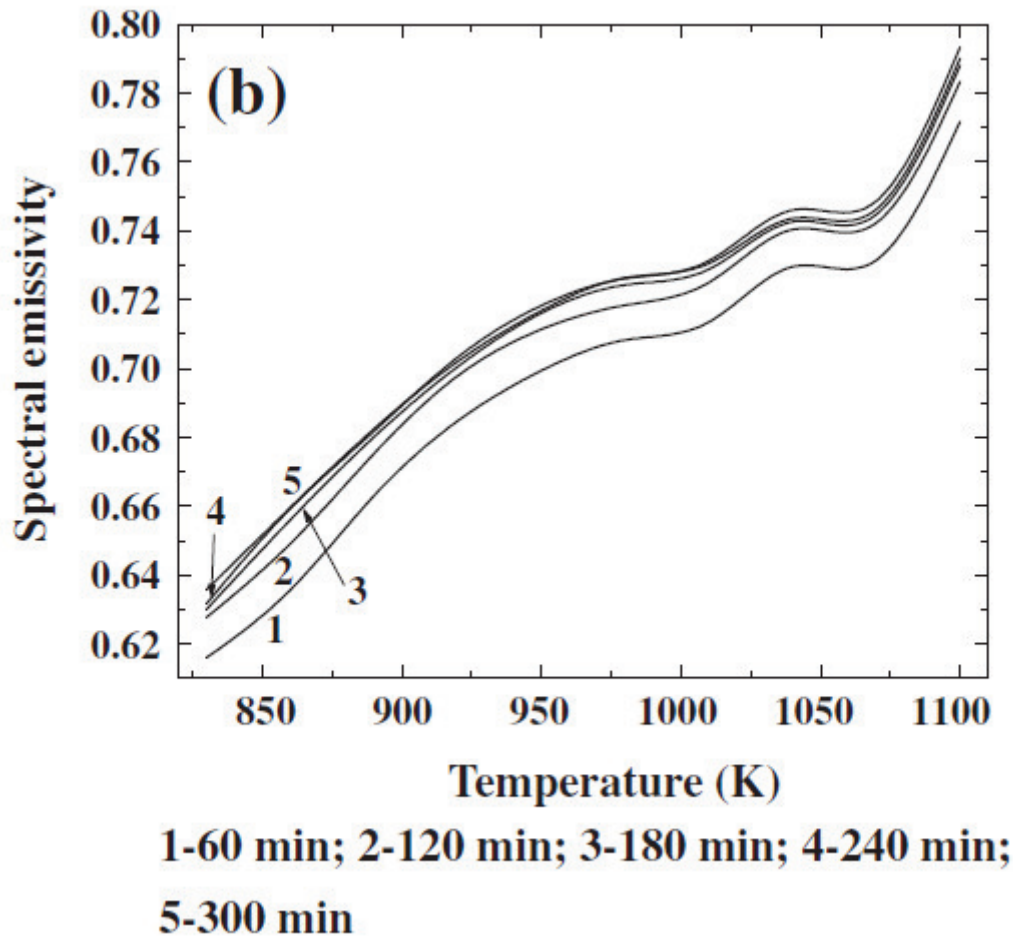

Figure 6. Temperature dependency of spectral emissivity, at 1.5 µm, for steel 304. The different graphs show the effect of heating-duration time, illustrated in more detail for 1100 K in Figure 5 (Shi, Zou, et al., 2014).

Combining the heat loss by radiation and those of convective cooling by small objects, the heat transfer of particles with the shape of a filament (250 µm) with a mass ranging between 1 to 1000 mg were computed for a semi turbulent scenario, i.e. 2300 < Re < 3300. The particles had an original temperature set to 1800 °C and were exposed to air at 30 °C. The temperature history of particles of various sizes is plotted in Figure 7 and it can be seen that the cooling of particles with a mass above 10 mg is generally quite small for times less than 0.25 s. Recall that the results are in total absence of particle oxidation which is a highly exothermic process that possibly can lead to heating of a particle should the oxidation process be fast enough and the surface-to-volume- ratio high.
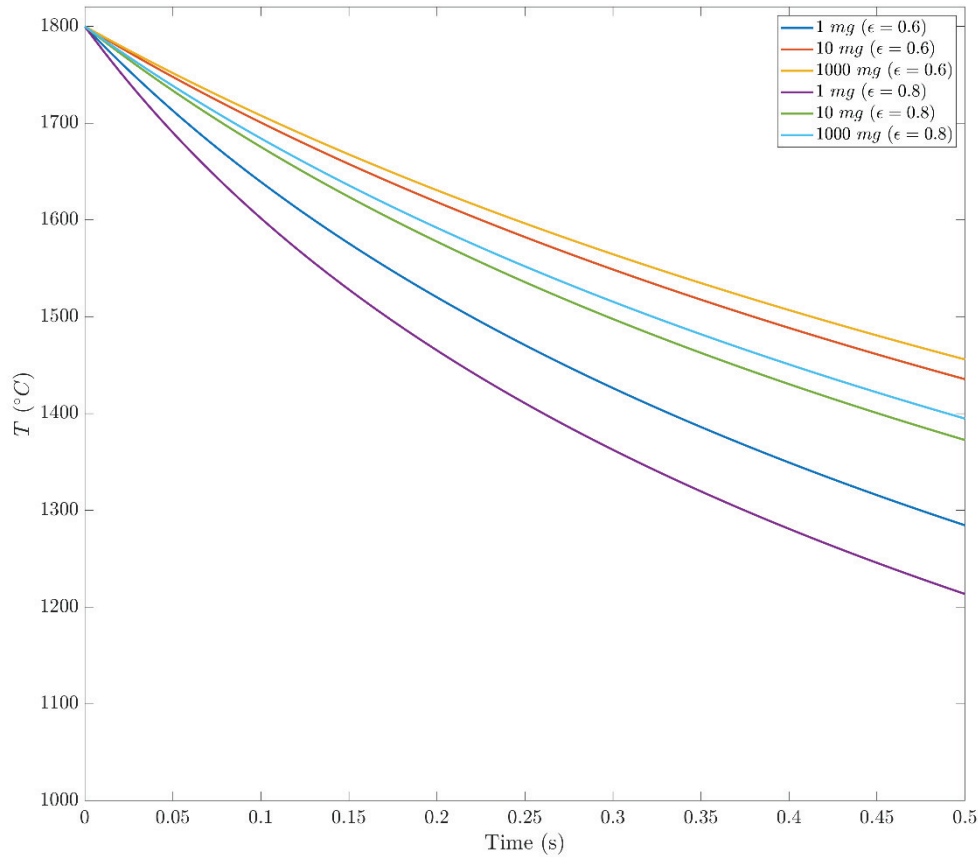
Figure 7. Temperature history of metallic particles of various sizes which original temperature was set to 1800 °C and are exposed to air at 30 °C for two emissivity values, 0.6 and 0.8.

1.2.2 Ignition by hot particles

Urban et al. investigated ignition by hot metal particles of a fuel bed consisting of cellulose particles with mean diameter 0.36 mm and average moisture content of 7 % (Urban et al, 2015). The metal particles were relatively large as compared to the sizes relevant for this study. The moisture content is equivalent to a fine fuel moisture code of 93.5, which occurs during very dry summer days. Four different materials were investigated: stainless steel, aluminium, brass, and copper. The result for stainless steel is shown in Figure 8. As can be seen the border between no ignition and ignition becomes less sensitive to particle temperature for larger diameter particles. The authors suggest that for small particles the particle energy is more important than the particle temperature since a small reduction in diameter requires a large temperature increase in order to uphold the ignition frequency. In general, both energy and temperature must reach certain thresholds in order to achieve ignition. The energy must be high enough to heat up the fuel so that enough pyrolysis gases are produced to achieve an ignitable mixture, and the temperature must be high enough, after losing energy to the pyrolysis process, to ignite the gas. The authors also make the observation that that melting of the particles plays a significant role for the ignition probability. For aluminum the latent melting heat correspond to an additional heating of the particle by 433 °C, which

corresponds to a considerable amount of energy that can contribute to pyrolyzate production.
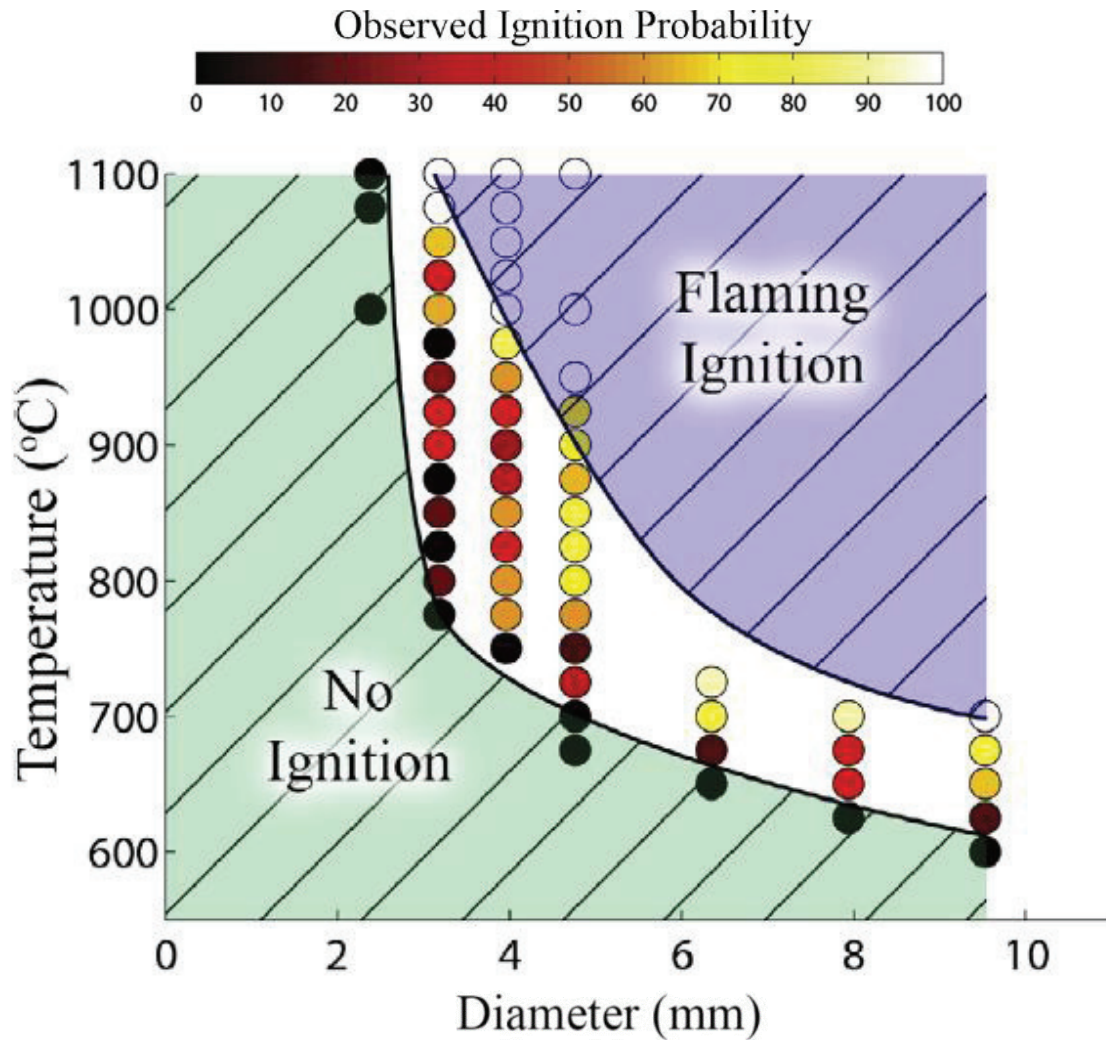

Figure 8 Ignition probability for stainless steel particles impinging on a bed of cellulose particles (Urban et al., 2015).

Hadden et al. (2011) utilized a variant of the so-called hot spot theory, developed by Gol'dshleger et al. (Gol'dshleger et al, 1973) in order to model experiments with 500 - 1300 °C steel particles 0.9 - 19.1 mm in diameter impinging on a fuel bed of dry fine-powdered cellulose. The hot spot theory by Gol'dshleger et al. constitute of set of equations where the parameter δ, the Frank-Kamenetskii hot spot parameter, must be approximated numerically. Based on these simulations and on thermophysical data for the cellulose and the steel particles Hadden et al. could qualitatively reproduce the experiments. The results are shown in Figure 9. One explanation for the quantitative deviations between theory and experiment presented by the authors is that the theory is based on the assumption that the particles become fully immersed in the fuel, whereas in reality they are often stuck on top of the fuel bed.
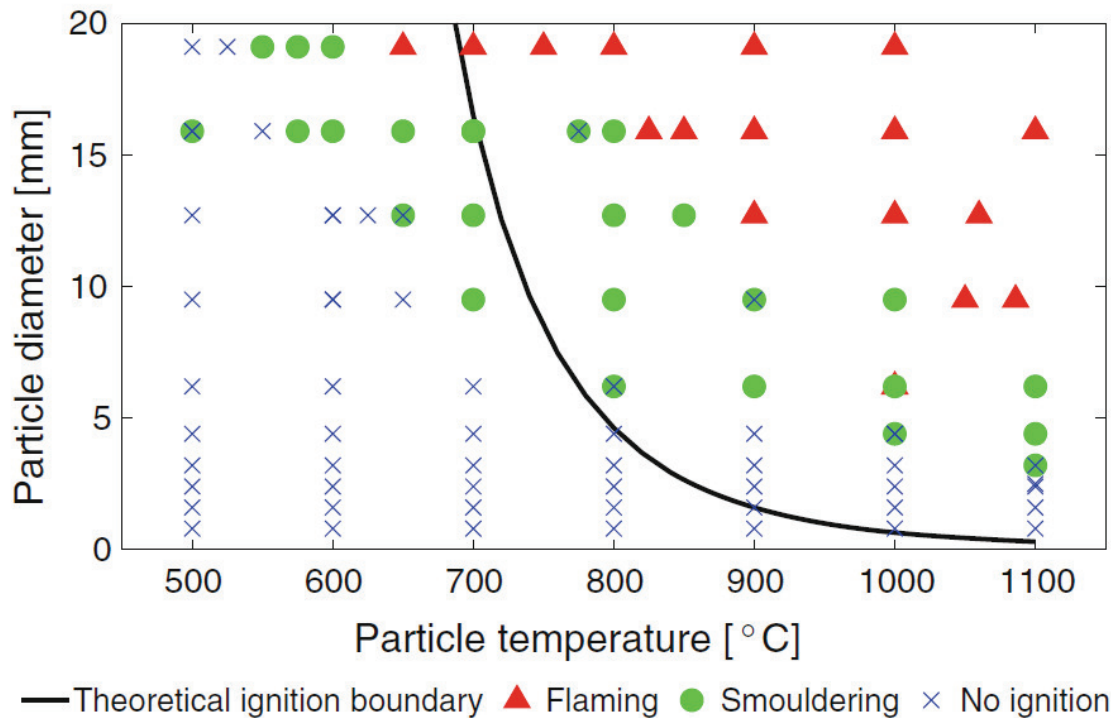
Figure 9 Comparison between ignition boundary based on hot spot theory and experimental results (Hadden et al., 2011).

1.3 Background summary

The background can be summarised by the following points:

- Heavy machinery ignites wildland fuels every year, leading to 20-50 annual rescue service dispatches. Compared to the large area that are covered by forestry machinery (estimated to ~490 000 ha/year) there are few ignitions but some of them have resulted in large spread and high consequences.
- Ignition seems to occur from heavy contact between hard steel and rock.
- New routines are implemented by the industry since 2017
- There is very little literature studying the phenomenon, but studies suggest that sparks from heavy machinery striking rock are not a viable source for igniting forest fuel
- When a fragment is deformed and throw off a large material the majority of the energy goes into the fragment itself and not the larger material.
- As new surfaces are exposed to air oxidation processes start. These are very rapid at high temperatures.
- The oxidation leads to even higher temperature, thus the fragment "burns".
- The fragment is also cooled by radiation and convection. Small objects cool faster due to higher convective transfer and higher volume to surface ratio. The emissivity of the particle is fairly constant in time and temperature.

2 Method

2.1 Generation of hot particles

We used a number of different methods to produce hot particles. A few of them were already established methods of igniting fuel such as a traditional fire steel or a modern fire-steel containing alkali metals and others were from heavy strikes between high strength steel and rocks.

2.1.1 Carbon steel fire striker

A classical carbon fire steel (Figure 10) was used to produce spark that we know traditionally are potent for igniting forest litter and could be assessed in the same manner as the other spark generators. It is a commercial product sold under the brand name Wilmas eldstål (2022). Hereafter the carbon steel fire striker is referred to as traditional fire steel. The steel was used against both granite and flint from Sweden by striking them as intended with our hands. The product was used to ignite cotton, dry moss and humus to verify the ignition potential.

Figure 10. A traditional carbon steel fire striker.

2.1.2 Modern fire steel – LightMyFire

Modern versions of the fire steel contain easily oxidizing elements of the lanthanide series: Ce 47.7 % and La 25.1 % as well as other elements such as Fe 24.4 %, Mg 0.9 % and Zn 0.65 % (by weight using XRF). It can produce hot sparks when struck or after being shaven by a knife or other sharp object. We used a commercial version called Swedish Fire Steel® sold by LightMyFire and is subsequently labelled LMF hereafter (LightMyFire, 2022). The LMF was used according to instructions with the associated steel scraper on dry grass, cotton, moss and humus and was also investigated using spectroscopy and high-speed camera imaging.

Figure 11. Swedish Fire Steel (LMF) from LightMyFire® used to produce sparks towards grass and humus.

2.1.3 Rotating Hardox

A metal disc for mounting on an angle grinder was cut from Hardox® 500, a wear parts steel grade produced by SSAB (SSAB, 2022) used for e.g. excavator buckets, wear sheet plates, wheel tracks and scarification discs. The disc was mounted on an angle grinder and forces against stones such as granite and flint to produce sparks used for temperature measurements. The sparks were also used for ignition tests on moss (*Pleurozium schreberi*, 5 % moisture) content and humus (10 % moisture content).
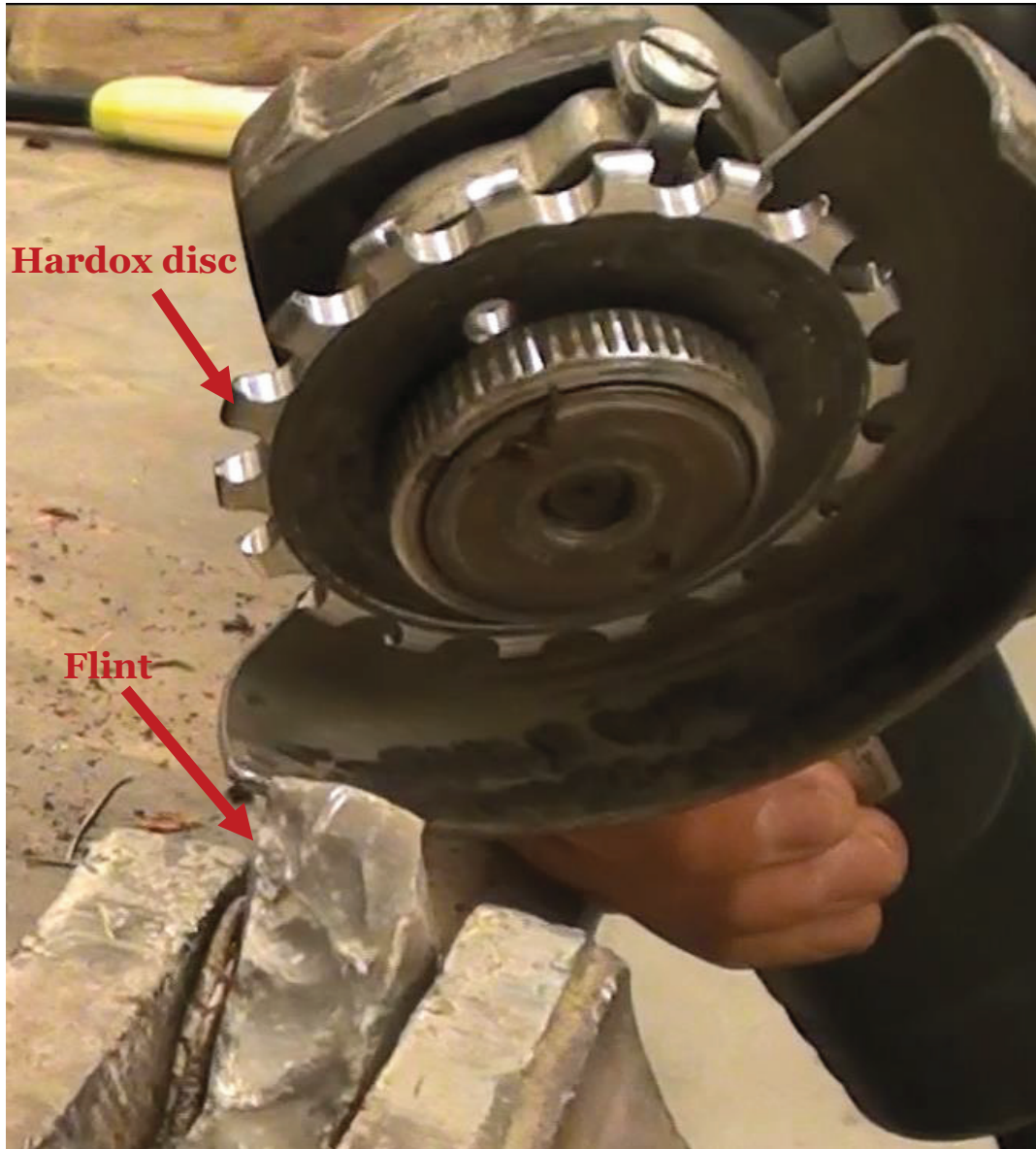
Figure 12. Hardox® 500 steel disc mounted on an angle grinder for temperature measurements and ignition experiments.

2.1.4 Rotating wheel of Hardox forced on granite

The rotatory multi-strike apparatus consisted of a flying wheel driven by an electric motor with eight Hardox heads colliding partially against a stationary stone which could be replaced on demand. The partial collisions against the fixed stone resulted in the production of glowing metallic fragments. The wheel rotated at a speed of 600 rpm (cutting speed of 10 m/s) with a normal force towards the rock of 200 N and thus created several strikes every second and therefore a more continuous production of sparks. Under the impact position a container of dry moss and humus was placed. Figure 13 shows a sketch and a photo of the rotatory multi-strike apparatus producing the fragments.
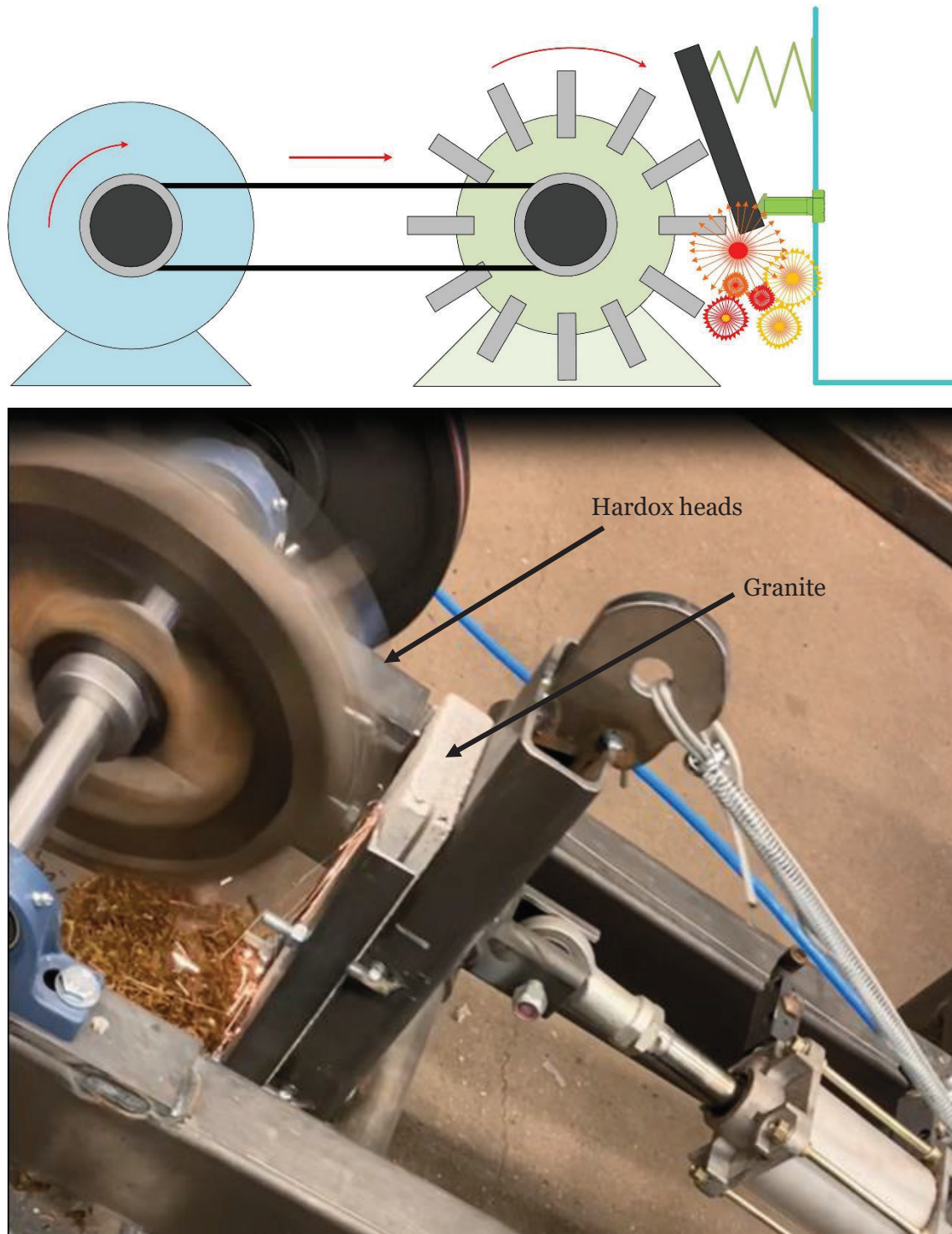
Figure 13. Upper: Sketch of the rotating wheel with Hardox heads against granite. Lower: Photo of the wheel while rotating 600 rpm producing glowing fragments.

2.1.5   Hardox and grinding belt

Hardox steel was forced against a running grinding belt using a force of 50 – 100 N to produce a continuous shower of sparks (Figure 14). The temperatures of the sparks were measured using the collimating lens which has a reduced field of view, improving the

spatial resolution. The measurements were taken at 31 distances from 13 to 970 mm from the grinding point. As such, the temperature variation along the shower could be measured. The velocity of the sparks was assessed using Particle Image Velocimetry (PIV) from video recordings of the sparks at 240 frames per second (see Appendix Figure 38). The average velocity field (Figure 39) thereafter resulted in a velocity to distance function (Figure 40) enabling us to calculate the average lifetime of the sparks at each distance from the grinding belt. The average temperature at each instance was corrected for the different emittance from particles at different temperatures calculated based on the mean and standard deviation of the temperatures from the fitted black-body spectra at each distance.

Figure 14. The shower of sparks from Hardox forced against a grinding belt.

2.1.6　Single strike axe testing machine

The single strike apparatus consisted of an arm coupled to a spring. The arm rotates on an axis and has a Hardox head which collides partially against a stationary stone which could be replaced on demand. When the arm of the machine is retracted, the spring becomes loaded, and the arm of the machine increases its potential energy. When the arm is released, the arm and its head accelerate and collides partially with a fixed stone resulting in the production of glowing fragments. Beside the impact position a container of dry moss was position to detect any possible ignitions should sparks land on the fuel. Figure 15 shows a sketch of the apparatus and photos of the setup during a strike.
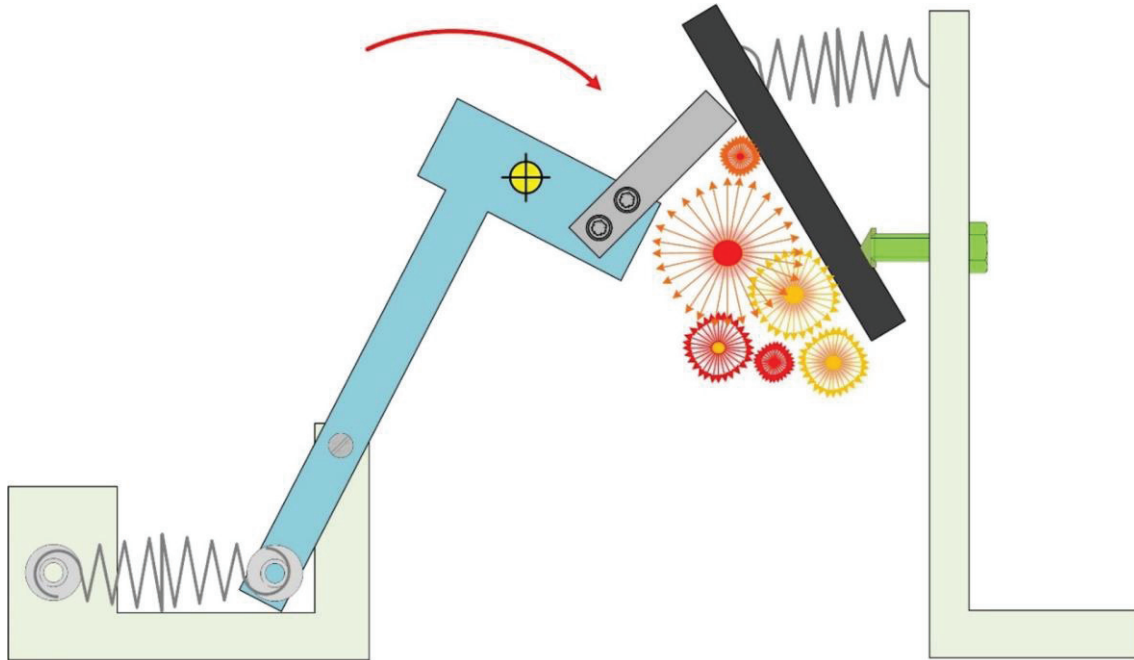

Figure 15. Upper: Axe testing equipment turned into a single strike apparatus producing glowing fragments of Hardox. Lower: Photo during (left) and just after (right) the strike.

2.1.7 Electrically heated metal shavings from turning

A filament of a specified material with a known thickness (between 50 and 250 µm) was set between two electrodes. A variable electric current (between 20 and 100 A) could run through the circuit, rapidly heating the metal to its melting temperature. After melting, the metal bubbles and spits leading to a filament breakage, where the high current forms a plasma under a very short time resulting in even higher temperatures where incandescent metal fragments are rapidly expelled from the electrode region. The process results in the production of large amounts of incandescent particles at temperatures above the melting temperature of the metal. The process is exemplified in Figure 16 (a) and (b), where (a) shows the filament before being heated and (b) when particles at temperatures above the melting temperature of the metal are expelled from the region comprehended between the electrodes.

Under the electrodes a container of dry (moisture content = 8 %) sawdust of 200 kg/m³ density. Fragments that landed in the sawdust container
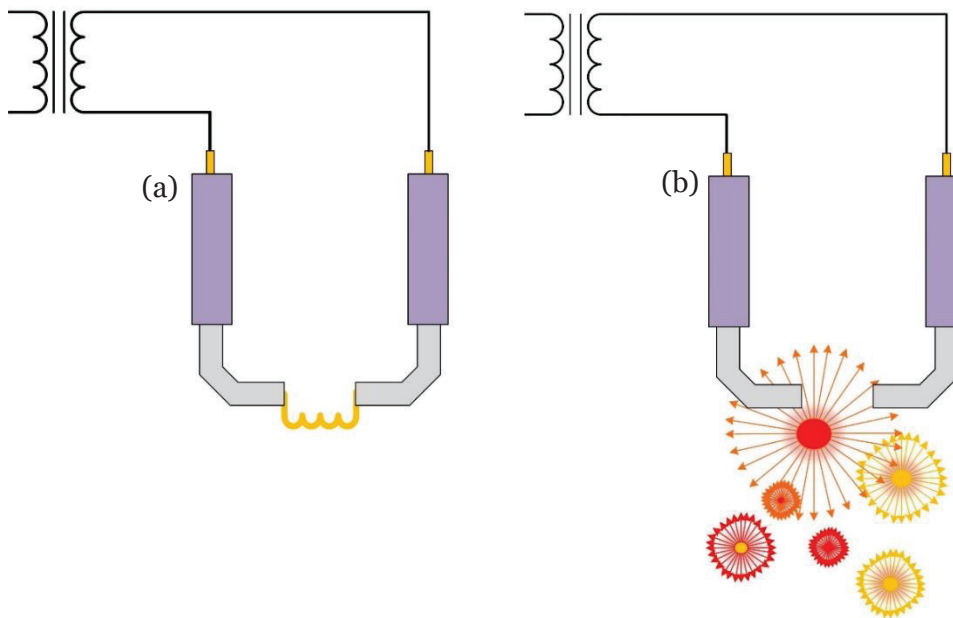

Figure 16. High current apparatus where a) shows the filament before being heated, and b) when particles at temperatures above the melting temperature of the metal are expelled from the region comprehended between the electrodes.

2.2 Temperature measurements

The emission spectra of the incandescent (glowing) particles were recorded using a grating spectrometer coupled to a fast detector with a spectral response ranging from 300 to 1050 nm (AvaSpec-ULS4096CL-EVO). The employed optics were made of CaF_2. The spectrometer and capturing optics were calibrated against a reference emission source (quartz-halogen lamp of type FEL with denomination F314 traceable to NIST). A sketch of the instrumentation employed for measuring the temperature of glowing particles is shown in Figure 17, where (A) denotes an incandescent particle which

electromagnetic emission is being detected by the coupling optics (B) and spectrometer (C).
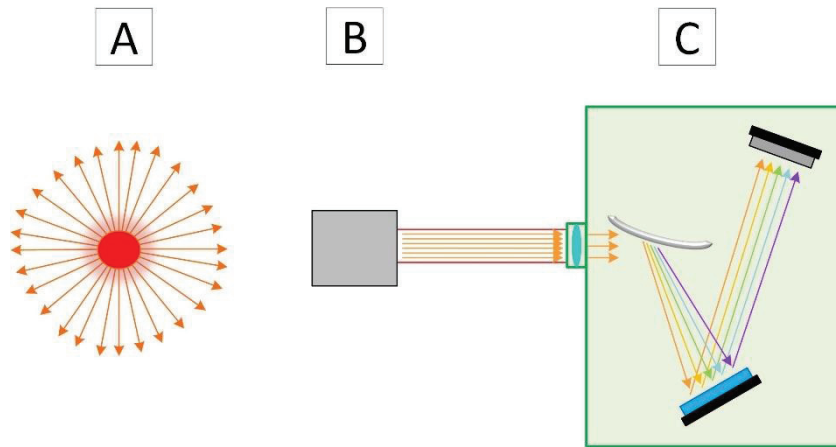

Figure 17. Instrumentation employed for measuring the temperature of incandescent particles where (C) denotes the grating spectrometer, (B) the coupling optics and (A) an incandescent particle which electromagnetic emission is being detected by the optics and spectrometer.

The temperature of the incandescent particles was measured by correlating their captured electromagnetic radiation against a set of Planck's distributions computed a priori and for a wide span of temperatures. The form of the curve from the captured electromagnetic emission was compared to the set of distributions using the minimum squares method. The accuracy of the method was tested against well-known sources, for instance, employing an incandescent halogen lamp excited at three voltages, a laboratory Black Body Radiator used as a national standard at RISE and a burning candle. Plots of the emission and measured temperature corresponding the halogen incandescent lamp are plotted in Figure 18 a-c. The resulting temperatures from the fitted spectra for the lamp excited at 6, 10 and 14 V are 1960, 2300 and 2570 K, respectively. The specified temperature for the lamp is 2600 K when excited at 14 V, rendering an error of 1.2 %. The optics and spectrometer were also subject to a black body radiation furnace for calibrating heat flux meters (see Appendix, Figure 29 for a photo). The furnace was set to 1173 K (900 °C) and the best fitted spectrum corresponded to a black body temperature of 1160 K, rendering an error of 1.1 % (Figure 18 d). The instruments were also applied to a burning candle, fitting the emitted spectra to 1640 °C (Figure 19).
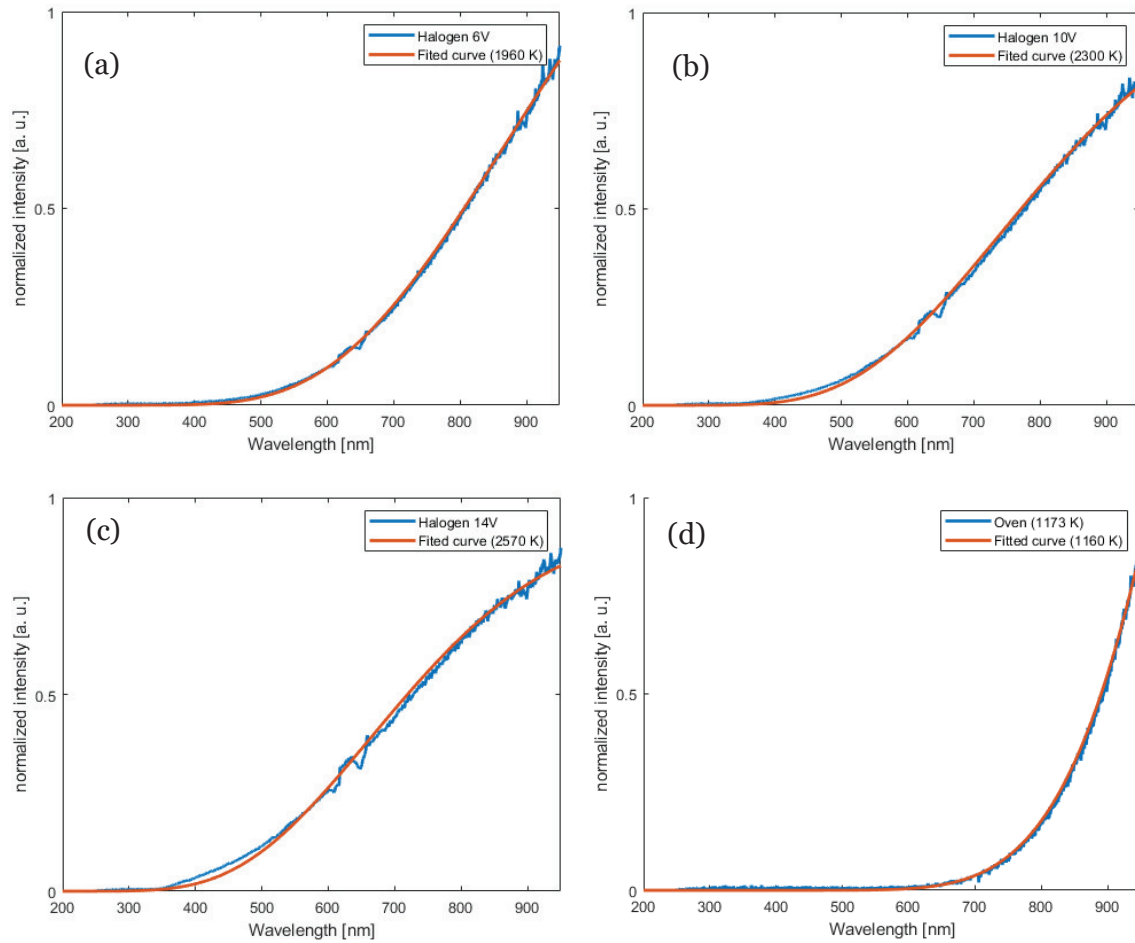
Figure 18. Emission from a halogen incandescent lamp excited different voltages and the corresponding fitted spectra from black bodies (a-c). The rated lamp temperatures for the different voltages are 6 V ~ 1950 K; 10 V ~ 2330K; 14 V ~ 2600 K. Also shown is the spectrum and fit from spherical black body calibration furnace for heat flux meters at 1173 K with the best fitted spectrum at 1160 K (1.1 % difference) (d).

The temperatures of the produced incandescent particles were measured using the method described above using a sampling time of 10 ms and at a frequency of 1 kHz. The temperatures were measured at the spots of interest using a collimator with a field of view of 18°.
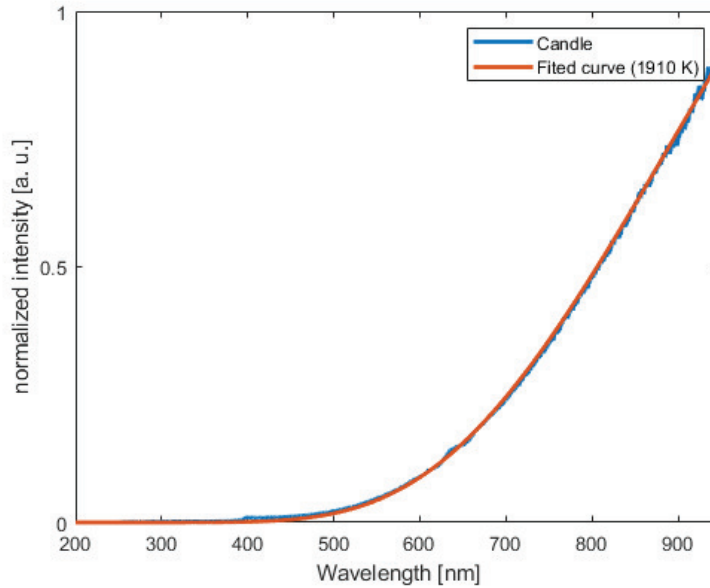
Figure 19. Emission from a burning candle and the fitted spectrum from a black body which temperature is 1910 K.

2.3 High speed camera

To determine fragment size, high speed imaging was applied to the rotating Hardox wheel, the modern LMF fire steel and the traditional fire steel. The camera was a Phantom 310 high speed camera operating at 800 Hz with a Nikkor Macro 105/1.8 objective. The focal length of the objective is thin so finding uncontrollable fragments in focus was a challenge. For LMF the possibility to use shadow photogrammetry increased the likelihood of spotting the fragments before they started to glow. This was achieved by placing a lamp with a diffusive film in the background of the image such that every object appeared through its shadow. This was not possible for the rotating Hardox wheel where fragments therefore only could be spotted if glowing.

3 Results

3.1 Fragment sizes in steel/rock strikes

The shadow photogrammetry performed on LMF strikes clearly shows the oxidation process of the fragments. One example is a fragment, visibly not burning, ejected from the LMF steel at what we label time = 0 ms. The fragment passes straight through the focus of the camera and the longer and shorter dimensions are determined to ~360 and ~160 µm, respectively. At t = 1.25 ms, an indistinct glow can be observed at the top of the fragment which is clearly visible at t = 2.5 ms. The heating from the exothermic oxidation yields a dramatic disintegration from t = 3.75 − 6.25 ms (Figure 20).
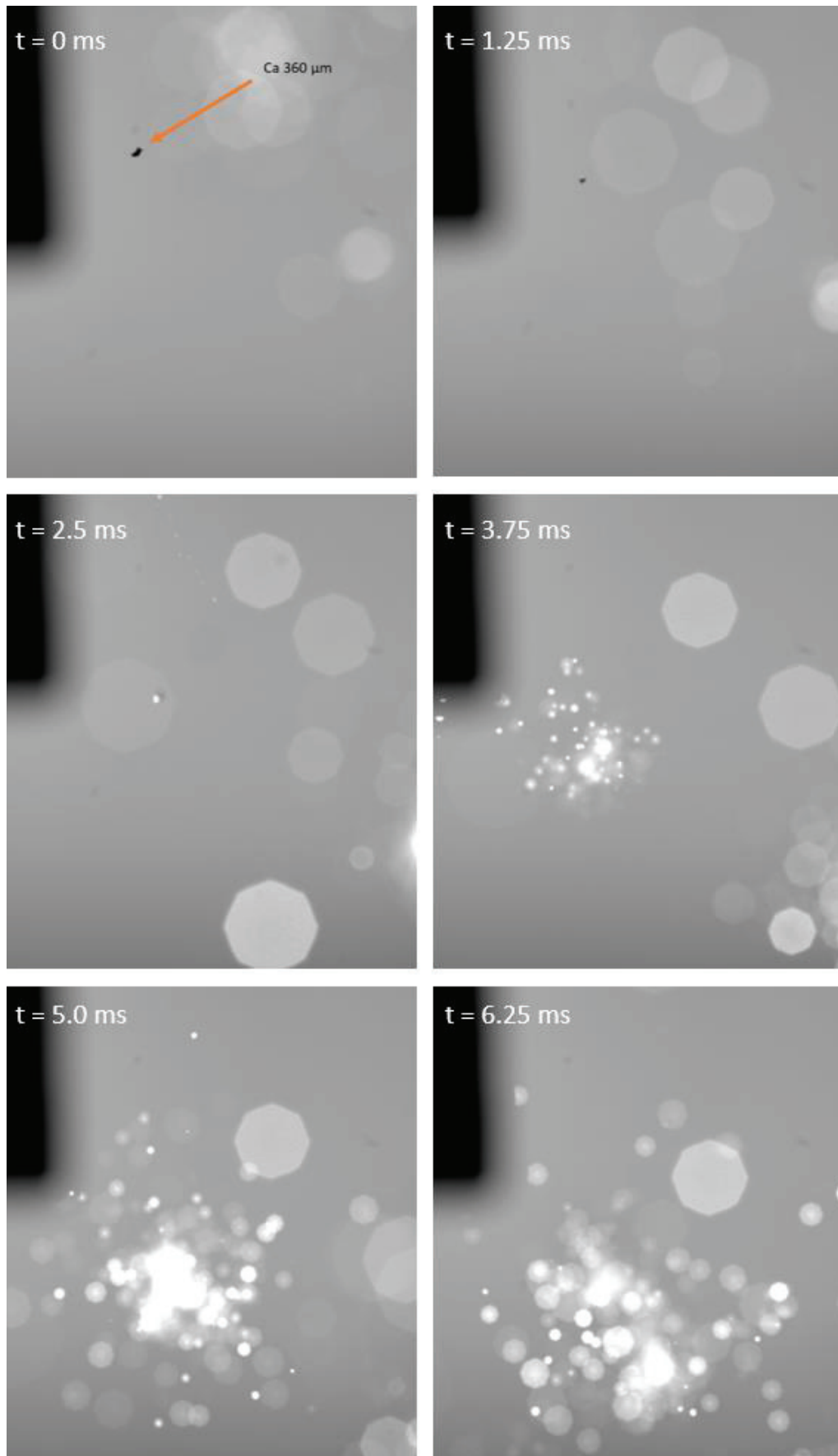
Figure 20. Shadow photogrammetric image sequence of sparks from LMF strikes. The upper right object is the LMF steel itself.
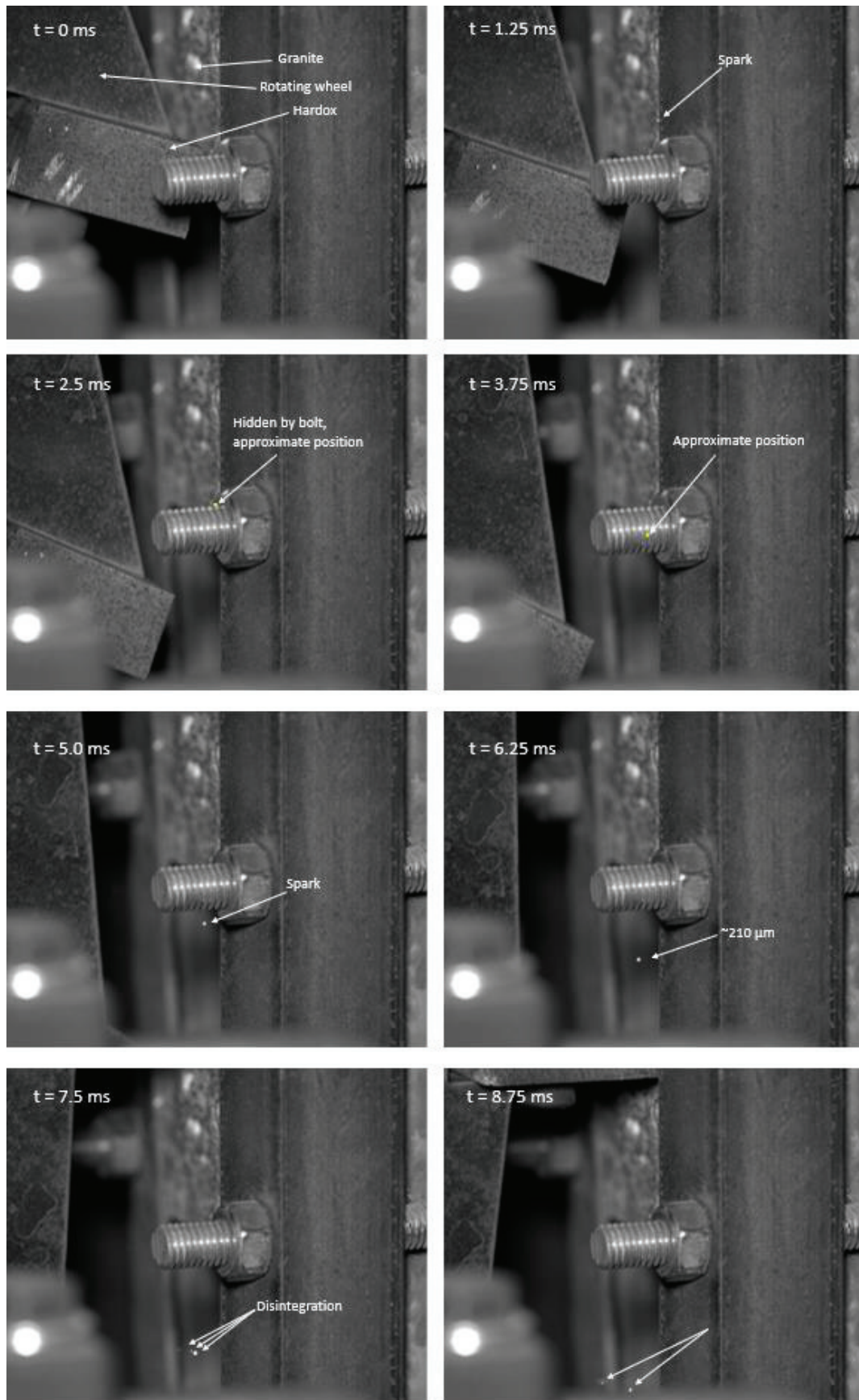
Figure 21. Image sequence of sparks from rotating Hardox wheel forced against granite. The last image is found enlarged in the Appendix (Figure 30)

Disintegration of fragments was also detected when assessing strikes of traditional fire steel and flint. These were more difficult to determine size from but are shown in the appendix (Figure 32)

For the rotating Hardox wheel against granite shadow photogrammetry was impossible but with normal photography we could capture glowing particles from the strikes although non-glowing fragments were very difficult to spot. One example shows a small glowing fragment visible at t = 1.25 ms in Figure 21 which is ca 2.5 ms after the Hardox stroke the granite. The fragment, temporarily hidden by a bolt, reappears at t = 5 ms and starts to disintegrate at 7.5 ms (Figure 21).
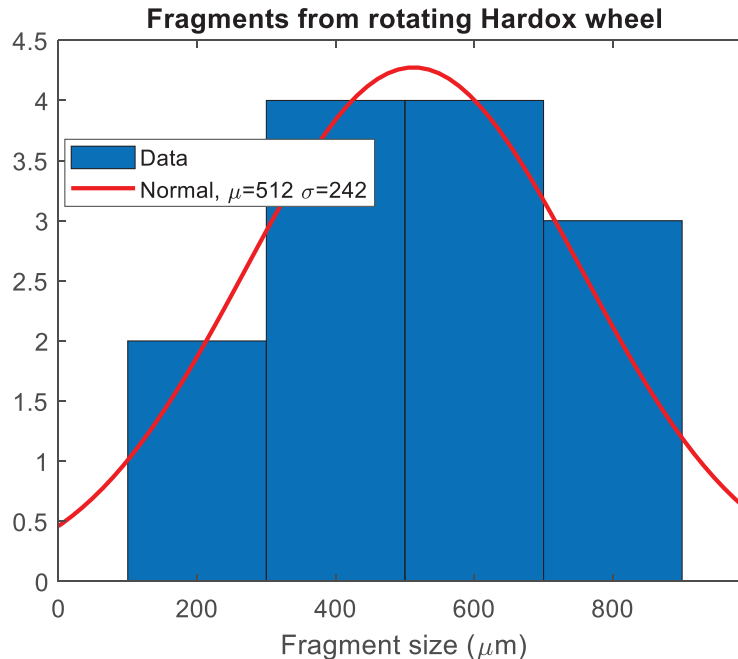

Figure 22. Distribution of 13 fragment sizes found using magnets after running the rotating Hardox wheel against granite.

After running the rotating Hardox wheel against granite the substrate moss was searched with a magnet to find residual fragments from the steel. 13 fragments were obtained, and their effective size (average of short and long distance) was determined using microscopy. The fragments were between 120 and 900 μm averaging at 500 μm (Figure 22), thus, in the same order of magnitude as that estimated from the high-speed camera recordings (Figure 21). It should be noted that also larger fragments (2 − 3 mm) were collected below the rotating Hardox wheel but it is not clear if these also were subject to high temperatures.

3.2   Temperatures in steel/rock strikes

Examples of fitted spectra from the fire steel and from LMF are shown below. Each spectrum from the fire steel exhibits a more uniform blackbody temperature compared to those of LMF which, however, provide a fair blackbody fit as well (Figure 23).
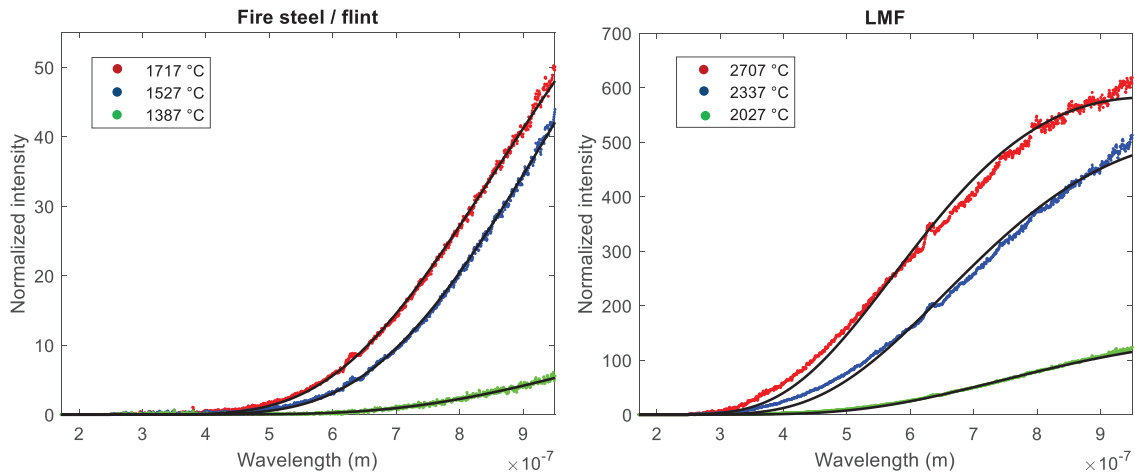
Figure 23. Examples of spectra with different fitted blackbody temperatures for flint to fire steel strikes (left) and LMF sparks (right).

The distributions of temperatures recorded (one from each successfully fitted spectra) for the sparks in strikes between flint and fire steel can be approximated by a normal distribution, $f(T) = \frac{1}{\sigma\sqrt{2\pi}} \exp\left(-\frac{1}{2}\left[\frac{T-\mu}{\sigma}\right]^2\right)$, averaging at 1521 °C and with a standard deviation of 120 °C (Figure 24). These represent the temperatures of all fragments from the strikes, both freshly produced and those that have travelled some distance from the point of the strike. The hottest spectra recorded is 1767 °C hot. The sparks from LMF are much hotter and we find two peaks, one at 2073 °C and a more significant one at 2512 °C (Figure 24). The spectra with highest fitted black body temperature was at 2847 °C.
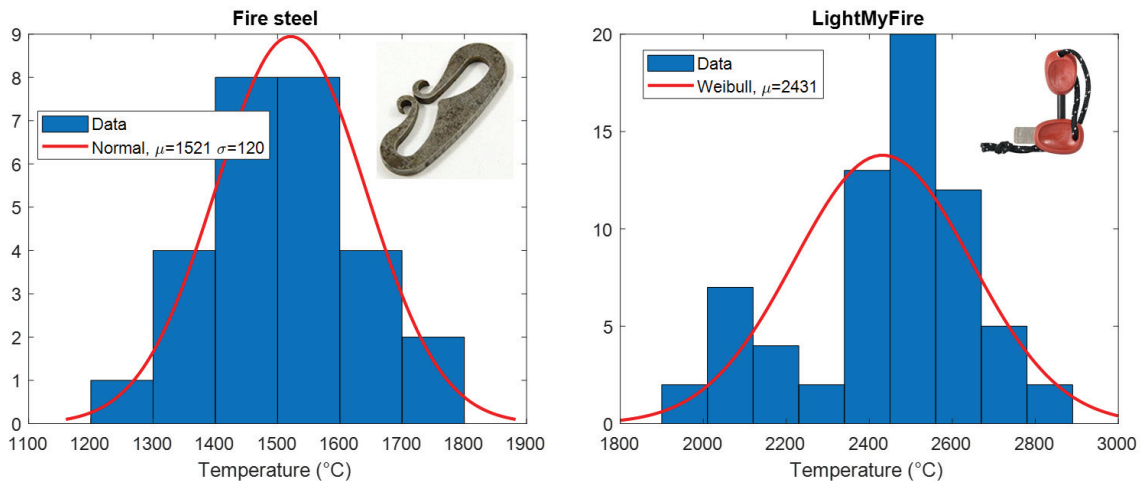

Figure 24. Distribution of temperatures recorded from sparks of fire steel and flint strikes (left) as well as from the LMF kit (right).

Distributions for temperatures of sparks from Hardon against granite in both the axe testing equipment and the rotating wheel exhibit maximum values for temperatures above 1600 °C. The spectra with the maximum temperatures were 1850 °C and 2020 °C for the axe testing and rotating wheel, respectively (Figure 25). The difference between which rock is involved is shown in the lower panels of Figure 25 where Hardox mounted on an angle grinder is forced against either granite or flint. When flint is involved in the strike the sparks are roughly 200 °C hotter than when the impact is against granite.
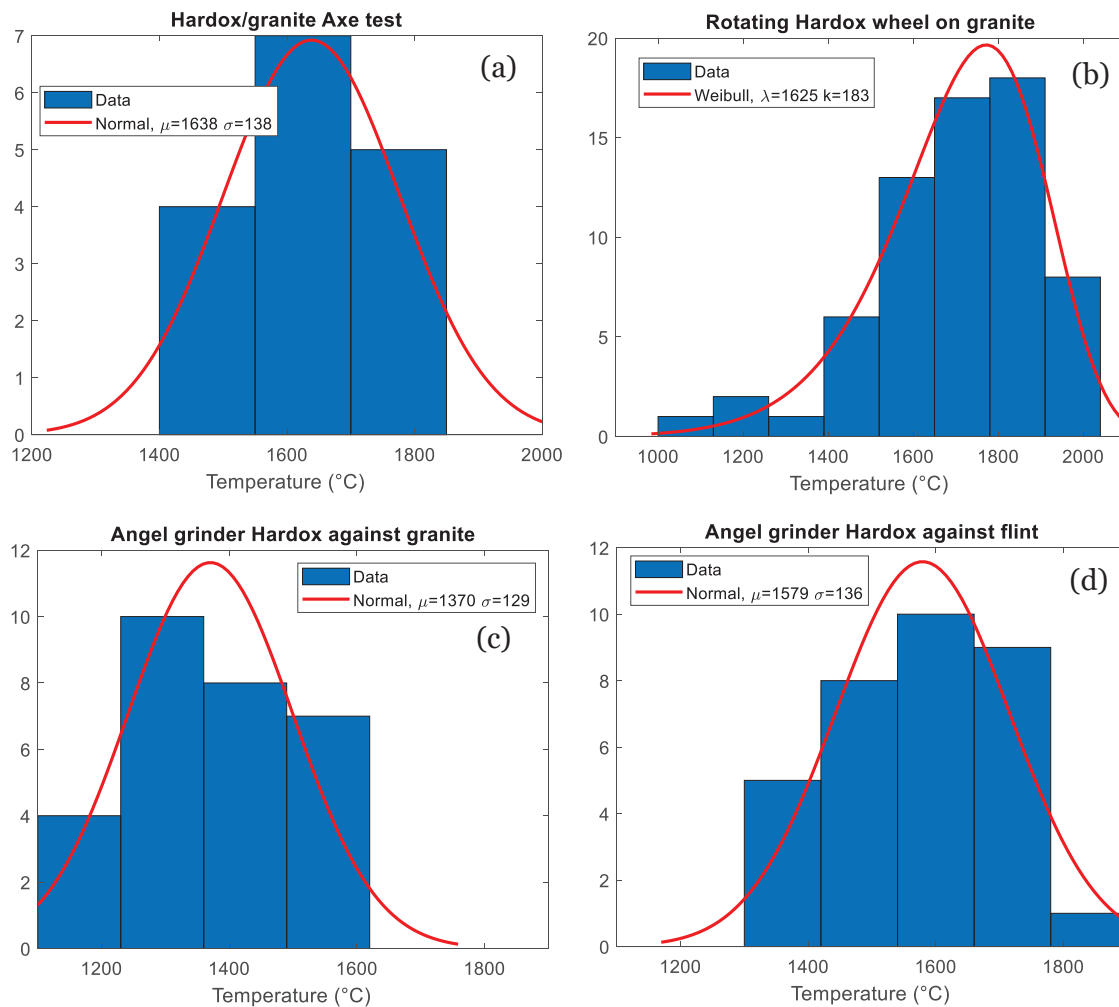
Figure 25. Distribution of temperatures recorded from strikes between Hardox and granite: (a) in the axe testing equipment; (b) from the rotating Hardox wheel forced against granite. The distribution of temperatures from the Hardox wheel is fitted with a Weibull distribution: $f(T) = \frac{k}{\lambda}\left(\frac{T}{\lambda}\right)^{k-1} e^{-\left(\frac{T}{\lambda}\right)^k}$. Lower panels show Hardox mounted on angle grinder forced against (c) granite and (d) flint.

The same technique for temperature determination was also performed for the electrically heated metal shavings. Results thereof are shown in section 3.3 Ignition experiments.

3.3 Temperature evolution of steel fragments

The temperature evolution of sparks from Hardox forced (50 – 100 N) against a running grinding belt was measured at several distances along the spark trajectory. The temperature increased rapidly from 1500 °C at the moment of impact to 1890 °C after 15-20 ms (Figure 26). A short plateau is thereafter formed followed by a much slower cooling towards 1700 °C after 200 ms. The longer the progression of time the larger variation of the temperatures was found, indicated by the standard deviation at each instance.
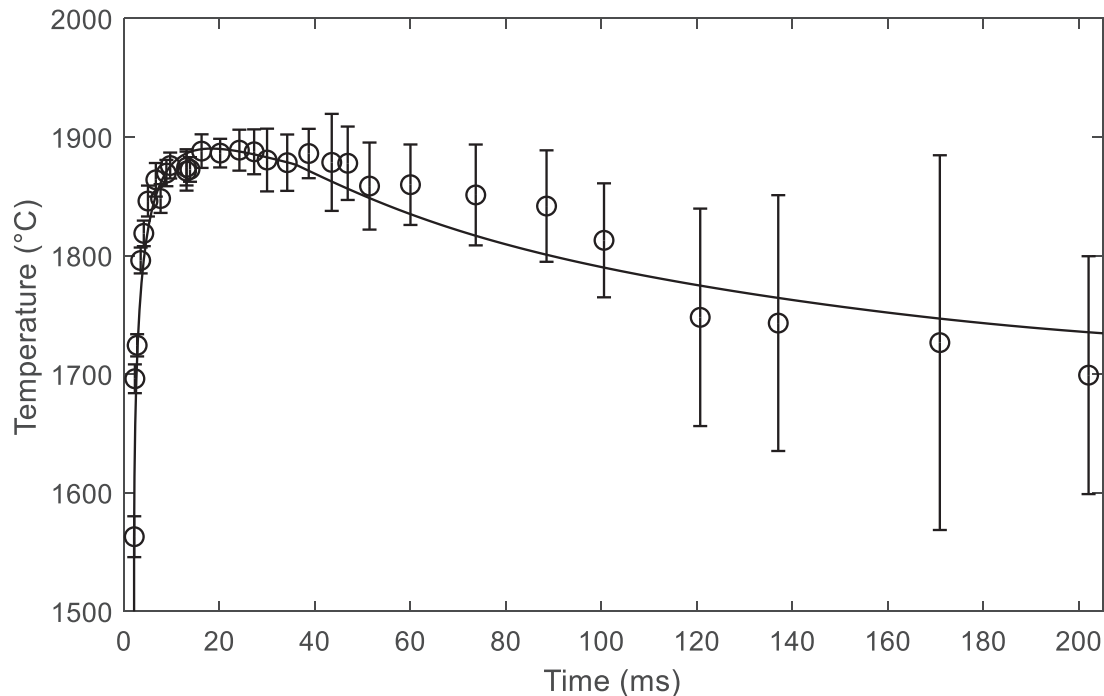
Figure 26. Temperature evolution of sparks in a continuous shower of Hardox sparks produced from a grinding wheel. The errorbars indicate the standard deviation of temperatures measured at each instance.

3.4 Ignition experiments

3.4.1 Fragments from metal to steel strikes

As expected, very easy ignition was obtained with the LMF fire steel on light materials. Dry cotton ignited repeatedly using only one strike and dry moss and grass ignited within a minute. Dry humus was a bit more difficult but ignited in glowing combustion after 5 - 10 minutes. The traditional fire steel against flint could also ignite dry moss but failed to obtain a sustained flame on grass even though individual straws glowed.

Hardox mounted on an angle grinder suffered from strong winds from the rotating wheel and the heat could not be contained in the fuel bed. Using granite, the sparks started smoke production in dry moss, but sustained ignition could not be recorded. Neither when flint was used could we detect any ignition with the angle grinder at full rpm. However, by turning off the grinder and forcing it harder against the flint while the Hardox disc rotated at ¼ speed the sparks started smouldering ignition in humus but no flames, even when the material was sprinkled with dust from the humus material. The same procedure on moss fuel also resulted in smoke production and smouldering while no ignition could be detected for grass or cotton.

The rotating wheel producing multiple strikes from Hardox and granite had a substrate of dry moss to investigate ignition. Also this setup suffered from the strong convection from the machine itself. In this case, the wind from the wheel was even stronger than for the angle grinder and sustained ignition was once again not possible to obtained. Smoke production and charred fuel was detected after the experiments but no remaining glow.

Table 1. Summary of ignition experiments on steel to rock strikes.

Material 1	Mat. 2	Fuel	Flaming ignition	Smouldering ignition	Comment
LMF	Steel	Cotton	1 sec	-	Every strike
		Moss	< 1 min	-	
		Grass	< 1 min	-	
		Humus	-	5 – 10 min	
Fire steel	Flint	Moss	5 – 10 min	-	
		Grass	-	-	
Hardox	Granite	Moss	-	Smoke	Angle grinder, full speed. Strong convection
	Flint	Moss	-	-	
Hardox	Flint	Cotton	-	-	¼ speed angle grind.
		Grass	-	-	
		Moss	-	Smoke	
		Humus	-	Smoke	
Rotating Hardox wheel	Granite	Moss	-	Smoke and char	Blown out by strong convection

3.4.2   Electrically heated particles

Since it was intrinsically difficult to control the trajectory (and thus the final destination) of the sparks from metal to rock strikes as well as most methods suffered from strong convective flow from rotating parts which blew out ignitions before flaming could occur, more controlled experiments were performed in which metal was electrically heated, producing particles to temperatures recorded from previous strike experiments.

The electrically heated metal shavings used in these tests were characterized both with respect to size and to temperature. A container of sawdust was placed under the electrodes and when fragments landed in the sawdust any flaming or glowing combustion was recorded visually. The spectrometer equipment was applied to capture the falling metal fragments and when such attempt led to trustworthy spectra (i.e. increasing temperature during heating and cooling temperatures during falling) the temperatures of each fragment was recorded. For some cases the lens could not capture the hot zone and in those cases the temperature was assessed by the melting point of the metal (as determined from DSC – Appendix Figure 33) and the mass and area of the fragment, as determined by observations in microscope (Figure 27).

Density of the fragments were below the density of the steel ($7800 - 8000$ kg/m^3) due to voids in melted parts.
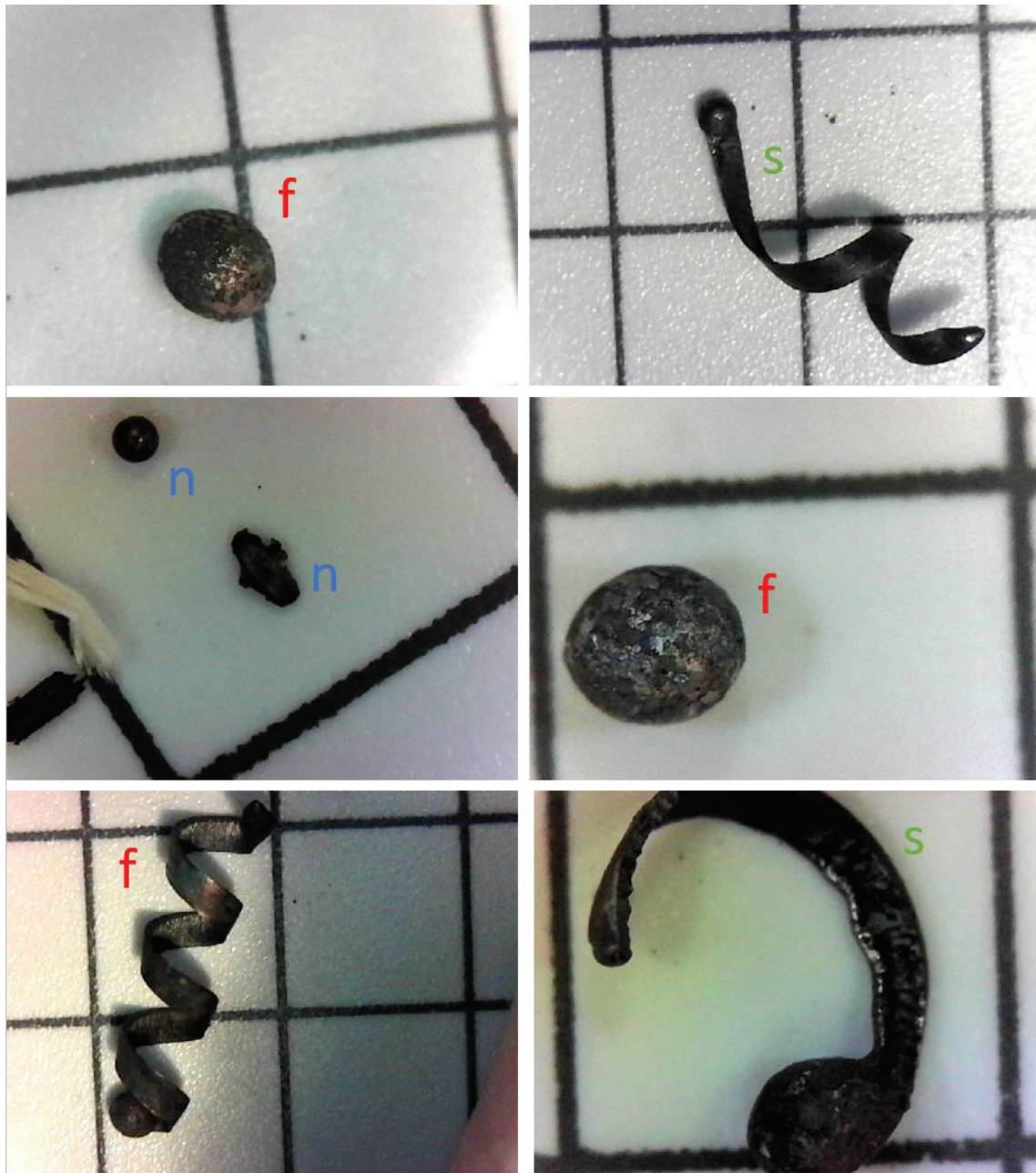
Figure 27. Examples of metal fragments from electrically heated ignition experiments. The lines are separated by 5 mm distance for reference. Letters refer to if the fragment leading to no flaming ignition (f), smouldering ignition (s) or to no ignition (n).
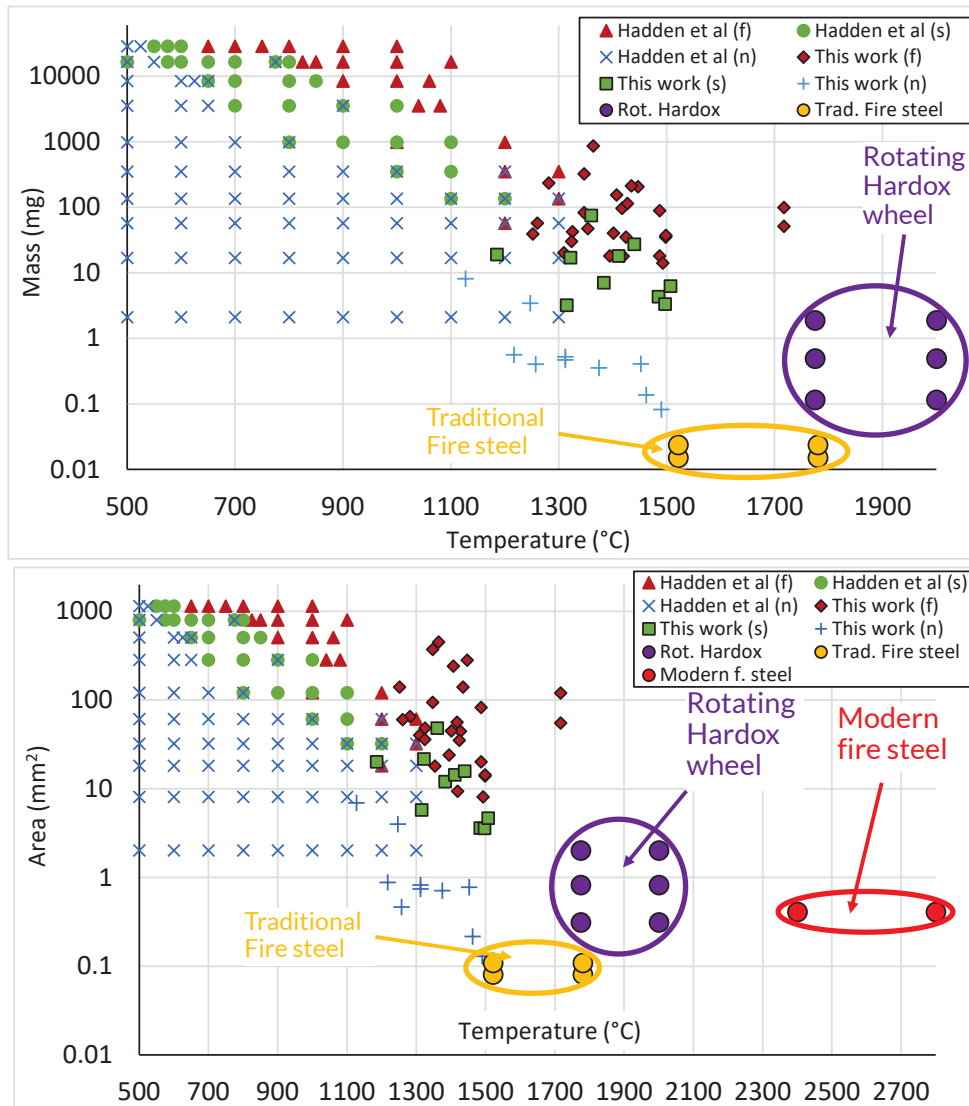
Figure 28. Mass (top panel) and area (lower panel) against fragment temperature for the three different ignition categories (flaming, smouldering and no ignition). The figure includes the results by Hadden et al (2011) as well as those from this work.

Charts of the fragments' temperature against fragment mass and area for each ignition category (flaming, smouldering and no ignition) was juxtaposed to the results by Hadden et al (2011) allowing us to continue the mapping of ignition to smaller fragments and higher temperatures (Figure 28). It is clear how the results from lower temperatures can be smoothly extrapolated to higher temperatures and that fragments with a temperature of 1400 °C can result in flaming ignition if the area is larger than 10 mm² or the mass larger than 10 mg. Smouldering combustion was obtained even for fragments as small as 3.6 mm² and 3.2 mg.

4   Discussion

What has become most clear during this work is how difficult it is to ignite forest litter with sparks when there is little control over temperature, size and trajectory of the fragments from the collision. There are many requirements for ignition to take place. If

the particle is both large and hot enough the actual position of it relative to the fuel is vital for ignition to occur. As the fuel characteristic on microscopic level is very heterogeneous the assessment of ignition potential requires a large statistical sample. Thus, this type of assessment is better done on a more homogeneous fuel such as sawdust or α-cellulose to reduce one unknown factor. Also, once a hot and large enough particle have found an advantageous position in the fuel a sustained ignition is also highly sensitive to external factors. These could be moderate convective flow in the very early stages of growth (once the fire stabilises, strong winds are almost always highly beneficial for high intensity). Perhaps this is one of the main reasons why so relatively few ignitions occur from strikes between hard metal and rocks.

However, this study shows that the temperatures of fragments originating in strikes from wear part metals (such as Hardox) and hard rocks (Figure 25), such as granite, are just as high or higher than those from traditional fire steel and flint (Figure 24). The temperatures of Hardox fragments after strikes with granite (10 m/s and 200 N normal force) average around 1630 °C in this study (depending on impact method) and some fragments exceed 2000 °C. This type of temperature increase is also supported by dimensional analysis on metal cutting (Figure 3) and from the colour of the sparks as captured by the naked eye of video camera. Also, the size of the fragments from these strikes are in the order of 500 μm, weighing about 1 mg (Figure 22). The temperatures and sizes of these fragments are also hotter and larger than what we find from similar analysis on strikes between traditional fire steel and flint.

The disintegration of fragments, as clearly noticed for modern fire steel, also occurs for fragments from the hard impact in the rotating Hardox wheel as for Hardox against the grinding belt. The fact that the disintegrating parts all glow, indicates that the fragmentation is preceded by rapid oxidation.

It is also evident that the oxidation of the steel becomes very rapid (Chen & Yuen, 2003) and essentially results in a burning of the metal fragment. This exothermic process explicitly appears as the temperature of sparks are measured as a function of the distance from the strike point. In only 15-20 ms the fragments heat up from the original temperature of 1500 °C to almost 1900 °C (Figure 26). After the highest temperature is reached the cooling process occurs much slower. In fact, only the average temperature measured at each point (circles in Figure 26) exhibits a reduction after 50 ms that cools the fragments by approximately 200 °c during 200 ms. The spread in the temperatures distribution at each instance increases simultaneously and the maximum temperature is therefore fairly constant (of slowly reducing) during the time it takes to travel the 1 m from the belt to the floor. From the snapshot of the spark shower, it appears that many of the fragments exhibit a disintegration process at some point whereafter their visibility quickly vanishes, probably due to the much faster cooling process of the smaller disintegrated fragments which exhibit both a higher convective heat transfer coefficient and a higher surface to volume ratio.

This study cannot determine the exact mechanism in the ignition processes. It could be speculated that disintegration of fragments within the fuel material would lead to a spatial concentration of the fragments with accelerated oxidation processes in a highly localized volume. As the cooling of the fragments just after disintegration is much higher, the heat transfer to the surrounding fuel thereby increases, possibly leading to ignition. A similar result could originate from a shower of sparks towards the same location. A

temporal delay could also lead to local pyrolysis ignited by following sparks. However, this hypothesis is speculative and the subject of further studies.

From the ignition experiments conducted on sawdust at temperatures above 1100 °C the trend from lower temperatures (as presented by Hadden et al) can be smoothly extrapolated to temperatures above 1500 °C and to smaller fragments (Figure 28). Given the fragment size and temperatures of Hardox to granite strikes, these sparks clearly exhibit the potential to ignite natural fuels, although the possibility of succeeding is low in real forests due to heterogeneous fuel characteristics.

The methods for generating fragments in this study differs from real impacts from e.g. heavy machinery (200 – 300 N normal force for the rotating Hardox and 50-100 N for the grinding belt). It could be argued that "real" impacts often have a larger normal force in the strike and possibly lower temperatures. This study shows that large force is a key component to producing both larger and hotter sparks and as such the results in this study would, although not being the exact same as that of a real heavy machinery, be situated on the conservative side of the spectrum for spark generation.

The results included in this work differ in great manner from the ones shown by Howitt (2015) with regard to the measured temperature of sparks and glowing metal shavings. In the present work, the recorded temperatures could reach 2000 °C, while in the work presented by Howitt, he estimated that the temperatures of glowing particles were around 500 °C. We believe the discrepancies in the measured temperatures originate in methodology differences between Howitt and this study.

Howitt employed a non-intensified infrared (IR) camera for estimating the temperature of these moving small particles. Infrared cameras estimate the temperature of an object by comparing the electromagnetic radiation emitted by the object in the infrared region (9~14 µm) against a calibrated source. In other words, the higher the temperature of an object is, the more infrared radiation it emits, and a higher radiation intensity is recorded. At larger wavelengths, the temperature of an object is almost proportional to the amount of emitted radiation. However, IR cameras require that the object is static with respect to the camera under the entire exposure time. If the object moves under the exposure time, just a portion of its radiation is registered by the exposed pixels of the sensor and its temperature is underestimated. This is most likely the case of the temperature measurements done by Howitt. Additionally, even though he described that the particles he measured were glowing, the temperatures he registered were far too low to be perceived as glowing by the naked eye. For particles to appear as glowing to the naked human eye, temperatures of nearly 800 to 1000 °C are needed.

Our group used another approach and decided to measure the temperature of the studied particles by register their radiation spectrally resolved using a fast spectrometer with short exposure times (< 15 ms).

Could there be a technical simple solution to reduce generation of potent sparks from heavy machinery? Our results indicate that harder rock yields warmer sparks (Figure 25) and that the same can be assumed for harder steel (Figure 3). The fragment size however decreases significantly with harder steel and the likelihood of generating sparks with enough potential is smaller for Hardox against flint compared to normal carbon steel against flint. Thus, exchanging wear part steel to less durable (i.e. less hard) material would most likely result in more frequent generation of potent sparks, in addition to the

cumbersome higher frequency of exchanging parts. Following the same arguments, harder steel would result in a lower probability of ignition but there are few materials that are practically (or economically) possible to use as replacement for the commonly used wear parts. There are also few parts under most machinery that consist of normal grade steel and there is therefore not much room for improvement using a material replacement strategy.

Instead, the spark generation found for heavy machinery is probably best handled as a fact and consequence of normal operations on forest land. The relatively few ignitions that occur are therefore in turn best handled by prepared operators with basic training in early-stage fire suppression, mandatory basic equipment on the machinery and routines for mitigation actions prior to the operations. The last item is highly important for sharing the responsibility of safe operations between landowners and contractors. Thus, the work initiated by the forestry industry resulting in guidelines for the industry (Skogforsk, 2017) should be developed for other types of non-forestry operation and should continue to be updated.

Possible future research regarding this topic includes the assessment of different steel types against different rock and possibly grading of the oxidation potential after the strikes. Also, understanding the effect of disintegration on the likelihood of ignition would be a large step forward for the knowledge on hot pot ignition processes.

5 Conclusions

This study shows that temperatures from sparks (metal fragments) created by impact between steel and hard rock can be assessed by a grating spectrometer coupled to a fast detector with a spectral response ranging from 300 to 1050 nm. This allows for studying the temperature evolution of such fragments and an assessment of their potential to ignite natural dead fuels. Size- and temperature distributions of sparks from modern and traditional fire steels as well as from strikes between wear part stell materials and granite or flint have been determined. The findings are summarized below:

- Strikes between strong wear parts metal and hard rocks produce sparks of metal fragments that are well over 1000 °C as they part from the mother material.
- These fragments exhibit a rapid oxidation process, further heating the particles. Examples in this study show a temperature increase of yet another 400 °C in 15 – 20 ms due to this process.
- The increasing temperature often leads to fragments exploding and disintegrating into several pieces.
- When such fragments disintegrate, additional unoxidized surfaces are created and a further increase in temperature can be expected. However, the smaller size and higher surface-to-volume ratio increases the heat loss rate. Thus, should this happen as the fragment is embedded in flammable light fuel this energy will quickly be transferred to the fuel, possibly leading to ignition.
- The disintegration process is extra fast and common in sparks from modern fire steel products (containing highly oxidating lanthanides) which easily ignites natural fuel.
- For harder rocks the temperatures of the fragments increase but the study does not perform a detailed quantification of the effect of hardness.

- Temperatures of normal fire steel against flint produces sparks with a temperature averaging at 1500 °C and with a maximum of >1750 °C.
- For strikes between granite and high strength wear part steel (Hardox 500) the fragments can be very hot if large forces are used in the strike (average 1630 °C and maximum >2000 °C). The temperature and size results in fragments with the potential to ignite dry natural fuels.
- Effective mitigating actions for forestry (or other types of heavy machinery operations in terrains) if not possible to use even harder steel, could be to accept these sparks as a natural consequence of the operations and focus on educated operators, suitable suppression equipment and to routinely review mitigating strategies prior to operations (such as driving on wetter/lower/less rocky lands during peak risk hours or -days.

6   Acknowledgements

7   References

J.K. Balch, B.A. Bradley, J.T. Abatzoglou, R.C. Nagy, E.J. Fusco & A.L. Mahood (2017) Human-started wildfires expand the fire niche across the United States, *proceedings of the national academy of sciences* **114**, 2946-2951.

Bodens Municipality, *Modern tids största skogsbrand*, Boden 2006, https://www.boden.se/db/web/filelib.nsf/0/D46F33F4AD73B525C12573590040EA4 A/$FILE/Branddokumentation.pdf (in Swedish, visited 2022-01-03).

C. Bryant (2008) *Understanding bushfire: trends in deliberate vegetation fires in Australia*, Technical and Background paper no 27Australian Institute of Criminology, Canberra.

Cal Fire - California department of forestry and fire protection (2015), Incident information, Via Stanley et al, 2020.

Campo, L. D., Pérez-Sáez, R. B., Esquisabel, X., Fernández, I., & Tello, M. J. (2006). *Rev. Sci. Instrum., 77*.

R.Y. Chen & W.Y.D. Yuen (2003) Review of the High-Temperature Oxidation of Iron and Carbon Steels in Air or Oxygen, *Oxidation of Metals* **59**, 433-468.

N.H. Cook (1966) *Manufacturing* Analysis, Addison - Wesley, Reading , Massachusetts.

A.C. Fernandez-Pello (2017) Wildland fire spot ignition by sparks and firebrands, *Fire Safety Journal* **91**, 2–10.

I. Finnie (1956) Review of the Metal Cutting Analyses of the Past Hundred Years, *Mechanical Engineering* **78**, 715.

Furukawa, T., & Iuchi, T. (2000). Experimental apparatus for radiometric emissivity measurements of metals. *Review of Scientific Instruments, 71*(7), 2843-2847. doi:10.1063/1.1150701

U.I. Gol'dshleger, K.V. Pribytkova & VV Barzykin (1973) Ignition of a condensed explosive by a hot object of finite dimensions *Fizika Goreniya I Vzryva,* **9**, 119-123.

R.M. Hadden, S. Scott, C. Lautenberger & A.C. Fernandez-Pello (2011). Ignition of Combustible Fuel Beds by Hot Particles: An Experimental and Theoretical Study. *Fire Technology,* **47**(2), 341-355. doi:10.1007/s10694-010-0181-x

D.G. Howitt (2015) An assessment of hot metal fragments from heavy mechanical equipment as a potential ignition source for forest litter. Journal of Fire Sciences **33**, 427–444.

K. Hyll, T. Johannesson & R. Björheden (2020*) På skogsbrandsfronten mycket nytt (Latest developments in forest fire research)*, Skogforsk Uppsala (in swedish).

M. Kobayashi, M. Otsuki, H. Sakate, F. Sakuma & A. Ono, A. (1999). System for measuring the spectral distribution of normal emissivity of metals with direct current heating. *International Journal of Thermophysics, 20*(1), 289-298. doi:10.1023/A:1021415305603

LightMyFire (2022) https://lightmyfire.com/se/swedish-firesteel-bio-army-2in1 (visited 2022-01-06).

M.E. Merchant (1945) Mechanics of the Cutting Process, *Journal of Applied Physics* **16**, 267 - 318.

K. Mikkelsen (2014) *An Experimental Investigation of Ignition Propensity of Hot Work Processes in the Nuclear Industry*. https://uwspace.uwaterloo.ca/handle/10012/8396

MSB – Swedish Civil Contingency Agency (2015) *Observatörsrapport: Skogsbranden i Västmanland 2014*, MSB798, Karlstad. ISBN: 978-91-7383-527-5 (in Swedish)

R. Ochoterena & M. Försth (2014) Pilot spark energy in the cone calorimeter: a source - of measurement uncertainties, *Fire and Materials* **38**, 760-764.

M. Omar, K. Kuwana, K. Saito & C. Couch (2007) The Use of Infrared Thermograph Technique to Investigate Welding Related Industrial Fires, *Fire Technology* **43**, 319-329.

A. Otsuka, K. Hosono, R. Tanaka, K. Kitagawa & N. Arai (2005). A survey of hemispherical total emissivity of the refractory metals in practical use. *Energy, 30*(2), 535-543. doi: https://doi.org/10.1016/j.energy.2004.04.019

J. Pujana L. del Campo R.B. Pérez-Sáez, M.J. Tello, I. Gallego & P.J. Arrazola (2007). Radiation thermometry applied to temperature measurement in the cutting process. *Measurement Science and Technology, 18*(11), 3409-3416. doi:10.1088/0957-0233/18/11/022

W. Sabuga & R. Todtenhaupt (2001). Effect of roughness on the emissivity of the precious metals silver, gold, palladium, platinum, rhodium, and iridium. *High Temperatures - High Pressures, 33*(3), 261-269. doi:10.1068/htwu371

M.C. Shaw (1985) The Theory of Metal Cutting. In: S.A. Tobias (Ed) *Proceedings of the Twenty-Fifth International Machine Tool Design and Research Conference*, Palgrave, London. https://doi.org/10.1007/978-1-349-07529-4_3

J.W. Shelton (1979) *Wood Heat Safety*, Garden Way, Charlotte VT.

D. Shi, Q. Liu, Z. Zhu, J. Sun, & B. Wang (2014). Experimental study of the relationships between the spectral emissivity of brass and the temperature in the oxidizing environment. *Infrared Physics & Technology, 64*, 119-124. doi: https://doi.org/10.1016/j.infrared.2014.03.001

D. Shi, F. Zou, S. Wang, Z. Zhu, & J. Sun (2014). Effect of surface oxidization on the spectral emissivity of steel 304 at the elevated temperature in air. *Infrared Physics & Technology, 66*, 6-12. doi:https://doi.org/10.1016/j.infrared.2014.05.001

J. Sjöström & A. Granström (2020) *Skogsbränder och gräsbränder i Sverige: trender och mönster under senare decennier*, Report MSB1536, Swedish civil contingency agency, Karlstad, ISBN: 978-91-7927-032-2 (In Swedish).

J. Sjöström, F. Vermina Plathner, A. Granström (2019) Wildfire ignition from forestry machines in boreal Sweden, *International Journal of Wildland Fire* **28**(9) 666-677.

Skogforsk (2017), *Riskhantering avseende brand vid skogsarbete – Branchgemensamma riktlinjer*, Skogforsk, Uppsala (in Swedish), https://www.skogforsk.se/cd_20210330165047/contentassets/c2426d933e2f4b8eaa2140362c83feda/riskhantering-avseende-brand-21-03-30.pdf (visited 2022-01-05).

SSAB (2022) *Hardox 500 - Wear-resistant steel with extra-high toughness*, https://www.ssab.com/products/brands/hardox/products/hardox-500 (visited 2022-01-05).

J. Stanley, A. March, J. Ogloff & J. Thompson (2020) *Feeling the heat: International perspectives on the prevention of wildfire ignition*, Malaga: Vernon Press. ISBN: 978-1-62273-828-1

J.L. Urban, C.D. Zak & C. Fernandez-Pello (2015). Cellulose spot fire ignition by hot metal particles. *Proceedings of the Combustion Institute, 35*(3), 2707-2714. doi:https://doi.org/10.1016/j.proci.2014.05.081

X.M. Viegas, M. Almeida, J. Raposo, R. Oliveira & C.X. Viegas (2014) Ignition of Mediterranean Fuel Beds by Several Types of Firebrands, *Fire Technology* **50**, 61–77.

C.-D. Wen & I. Mudawar (2004). Emissivity characteristics of roughened aluminum alloy surfaces and assessment of multispectral radiation thermometry (MRT) emissivity models. *International Journal of Heat and Mass Transfer, 47*(17), 3591-3605. doi:https://doi.org/10.1016/j.ijheatmasstransfer.2004.04.025

C.-D. Wen & I. Mudawar (2005). Emissivity characteristics of polished aluminum alloy surfaces and assessment of multispectral radiation thermometry (MRT) emissivity models. *International Journal of Heat and Mass Transfer, 48*(7), 1316-1329. doi:https://doi.org/10.1016/j.ijheatmasstransfer.2004.10.003

Wilma Naturprodukter (2021)
https://www.wilmanaturprodukter.se/produkt/eldstal/?v=f003c44deab6 (visited 2022-01-06)

VF. Zarko & A. Glazunov (2020) Review of Experimental Methods for Measuring the Ignition and Combustion Characteristics of Metal Nanoparticles, *Nanomaterials* **10**, 2008-2034.

Appendix A – Photos and additional figures

Figure 29. Visual photo of the spherical black body furnace used to validate the temperature measurements using spectroscopy. Photo shows the furnace exterior (metal grey) and the duct (orange) leading into the furnace interior (yellow) at 1173 K.
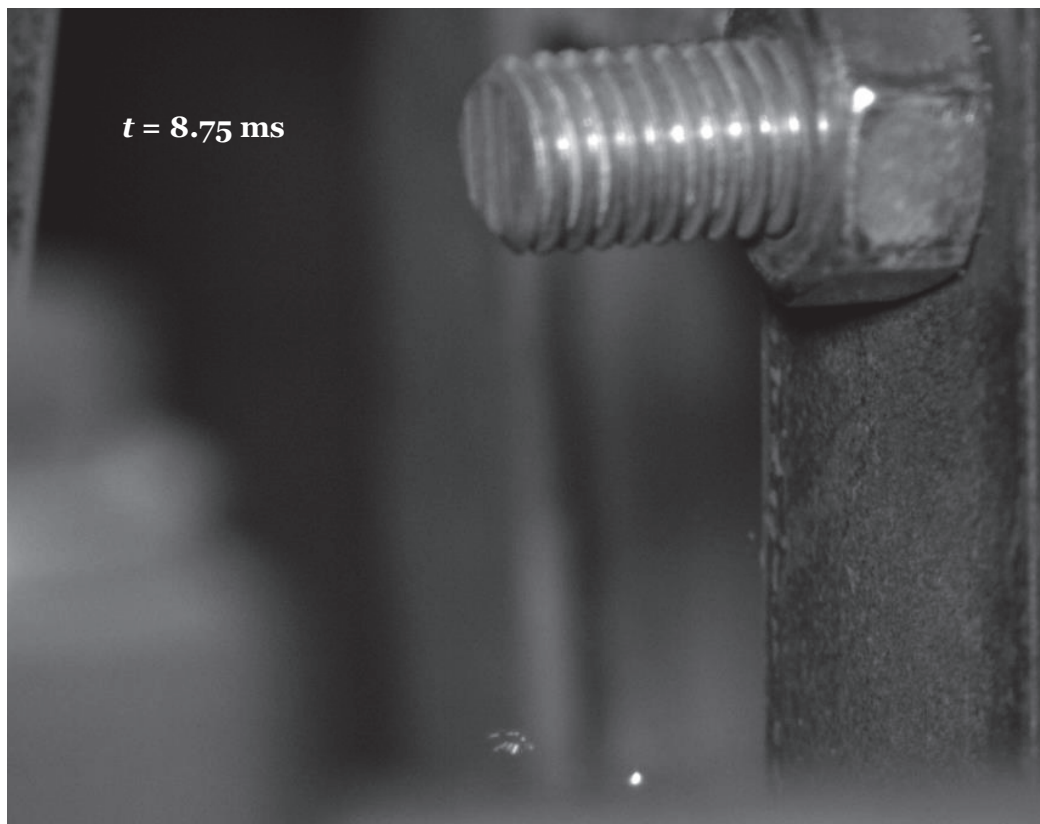
Figure 30. Enlarged photo of disintegrating spark from strikes between rotating wheel of Hardox and granite, c.f. Figure 21.
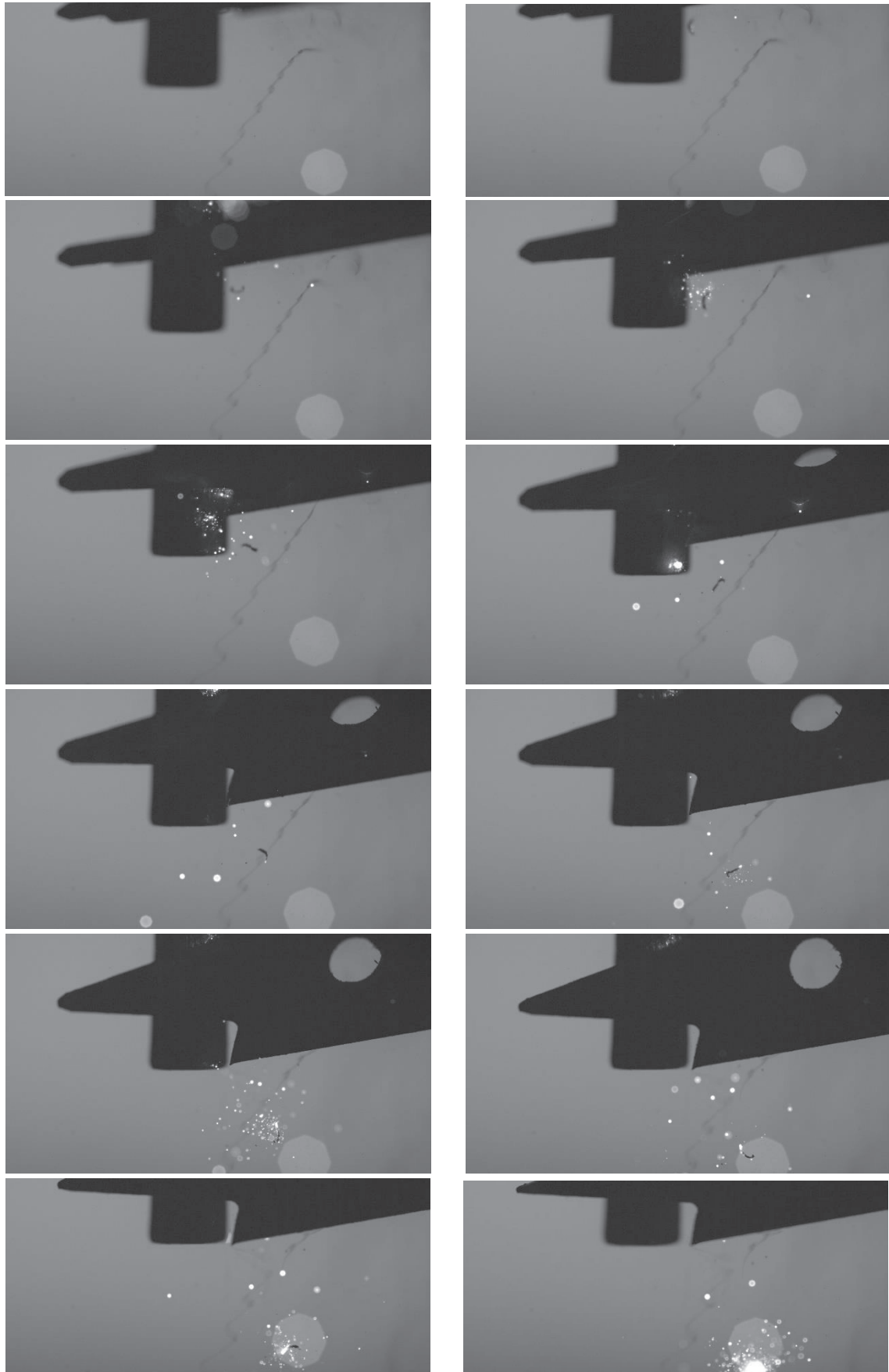
Figure 31. Shadow photogrammetry sequence of a large spark from LMF fire steel (Swedish Fire Steel®)
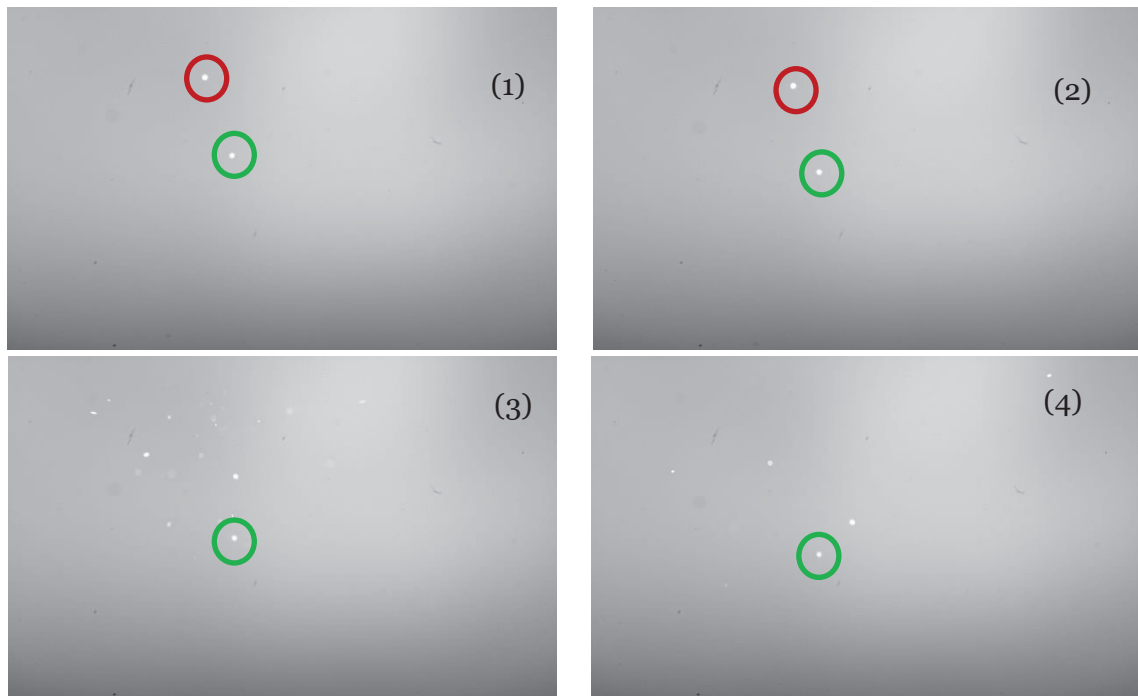
Figure 32. Photo sequence of sparks from strikes between traditional fire steel and flint. Note how the red labelled spark disintegrates into smaller fragments.
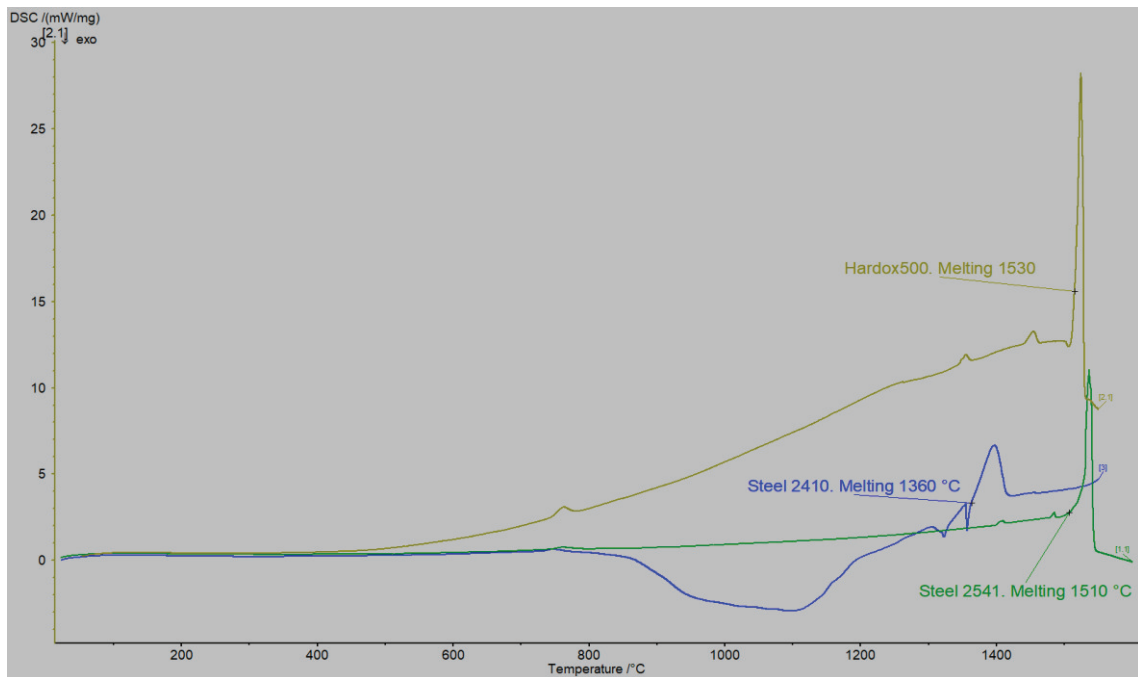
Figure 33. DSC thermograms of the three steel alloys used in the electrically heated fragment experiments identifying the melting temperature.
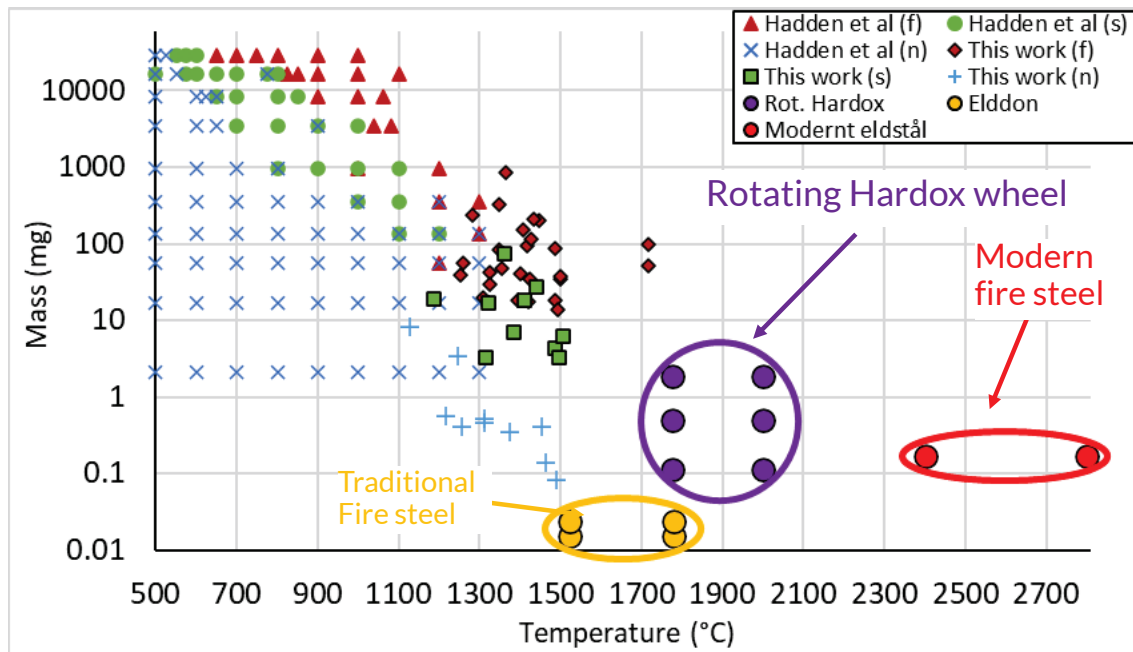
Figure 34. Same data as the lower part of Figure 28 using mass on the y-axis.
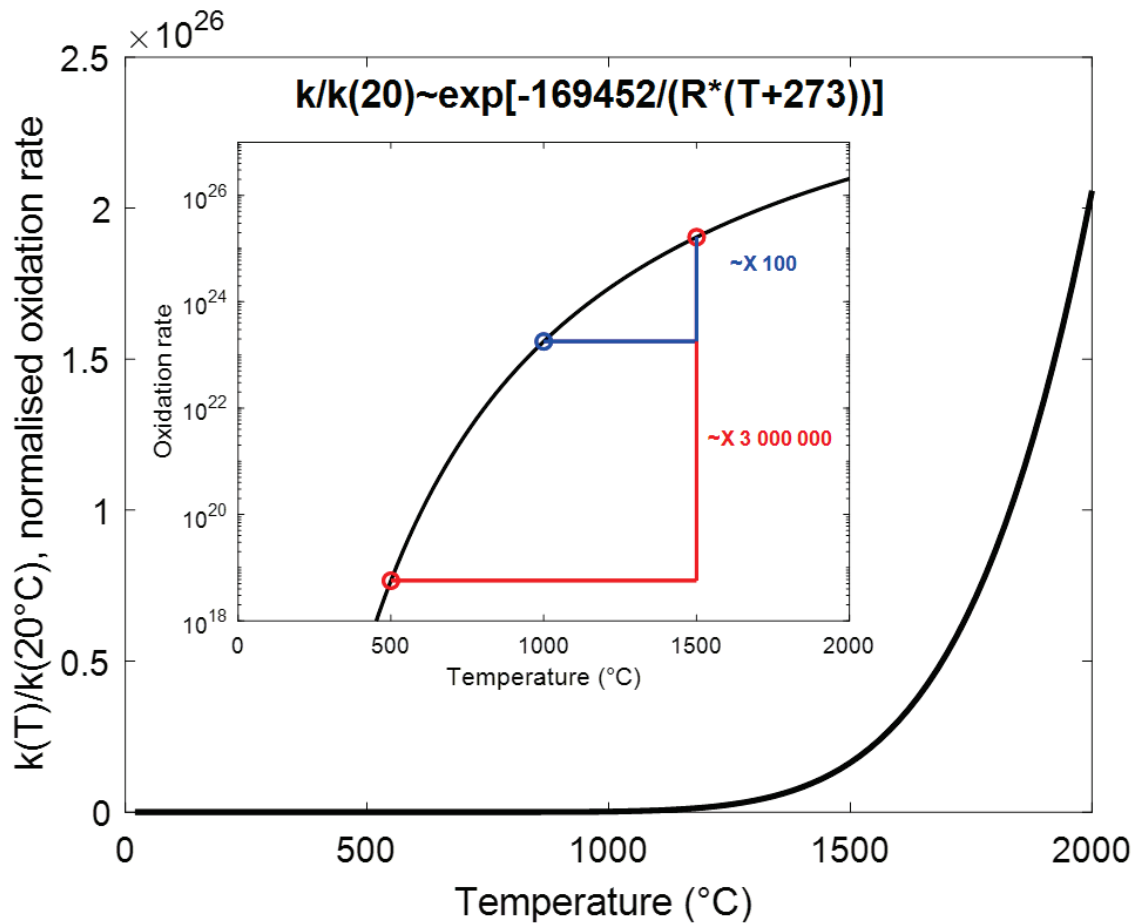
Figure 35. Oxidation rates of iron at high temperatures normalised to the rate @20 °C. The results are extrapolated from the experimental data from 600 – 1200 °C as per Chen & Yuen (2003). The inset shows the same data on a logarithmic y-axis.

Figure 36. Snapshots from the spark generation of the grinding belt used for temperature evolution of the fragments.

Figure 37. More snapshots from the spark generation of the grinding belt used for temperature evolution of the fragments.

Figure 38. PIV analysis assessing showing the video snapshot and the velocity of sparks (arrows) assessed from the previous snapshot.
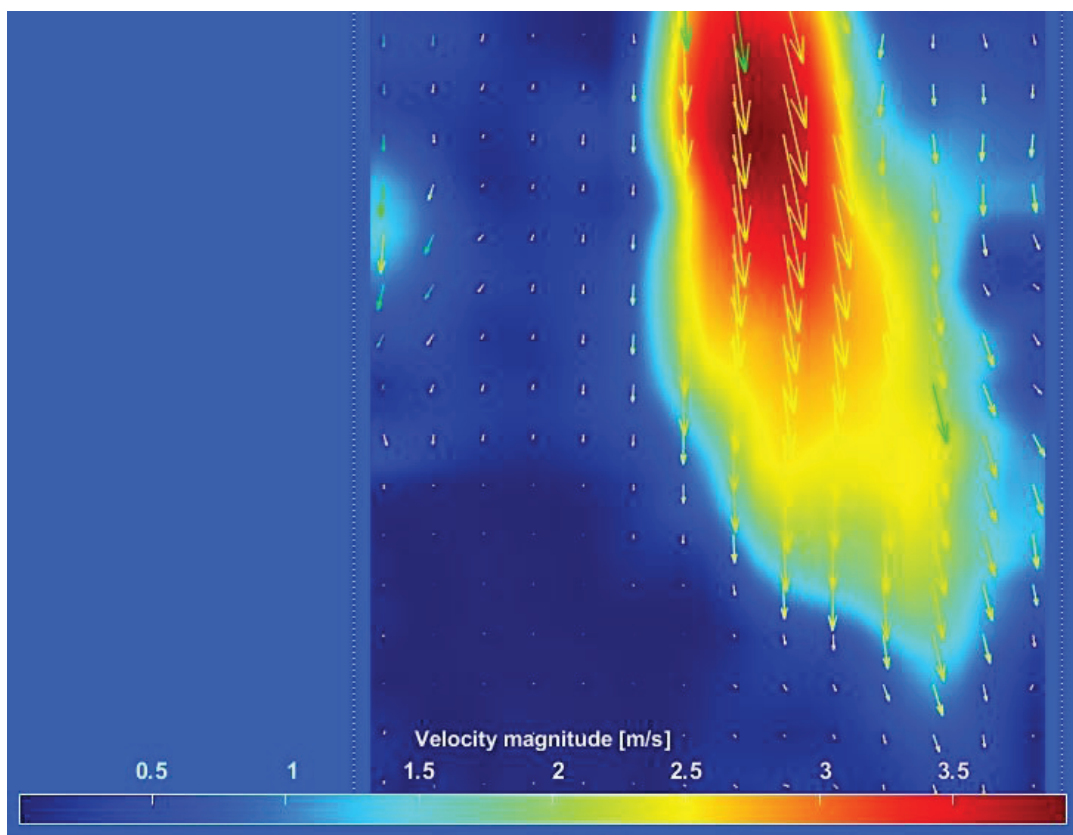
Figure 39. Average velocity field from assessment of 200 frames (as in Figure 38) from the video recording of the sparks produced by the grinding belt.
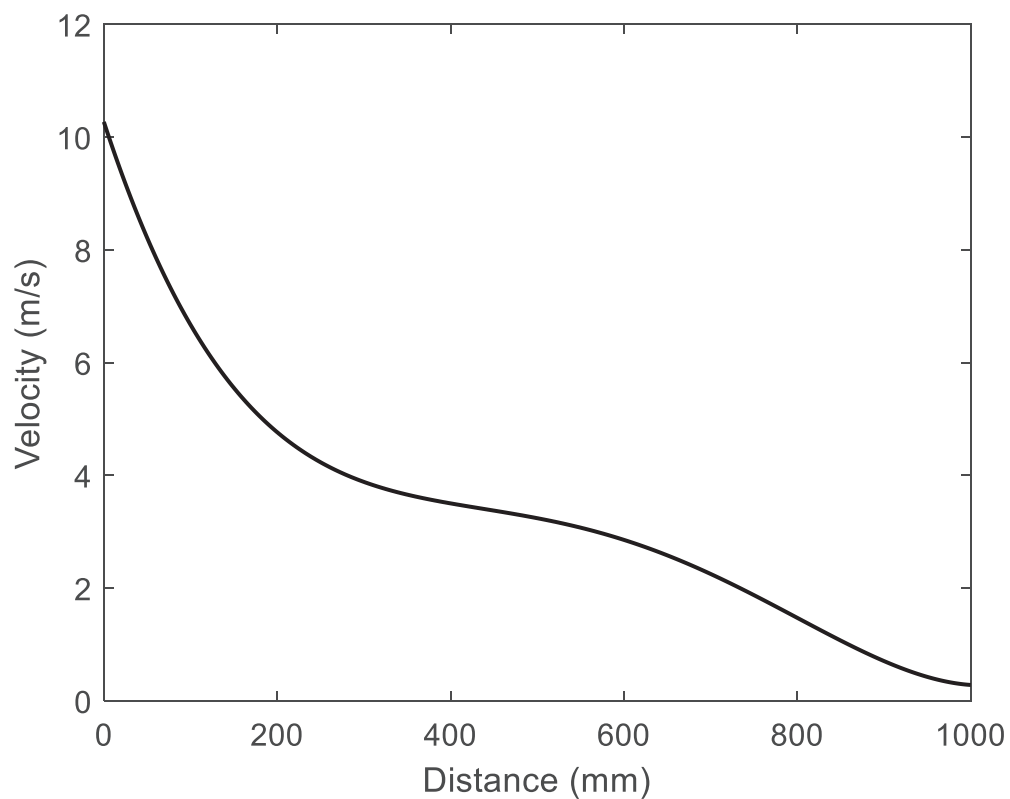
Figure 40. Average spark velocity (from Figure 39) as a function of distance from the grinding belt used to calculate the time from collision of the sparks in Figure 26.

Support organisations

This project was funded 2019 by the organisations below

The Swedish Fire Research Foundation - enables
development of fire safety knowledge by research and other activities,
and the spread of this knowledge to make a difference in our society.

This is possible trough raising money from all kinds of organisations with
fire safety on their agenda as well as for altruistic reasons. The broad
support from our society together with prosperous networks are key
factors for our success.

Our mission is **"A fire safe society built on knowledge"**

Brandforsk
info@brandforsk.se, www.brandforsk.se

Project team